

Surface Roughness Effects on Separated and Reattached Turbulent Flows
in Open Channel

by

Afua Adobea Ampadu-Mintah

A Thesis Submitted to the Faculty of Graduate Studies of

The University of Manitoba

In Partial Fulfilment of the Requirements of the Degree of

MASTER OF SCIENCE

Department of Mechanical and Manufacturing Engineering

University of Manitoba

Winnipeg, Manitoba

Canada

Copyright © 2013 by Afua Adobea Ampadu-Mintah

ABSTRACT

An experimental research was performed to study the effects of surface roughness on the characteristics of separated and reattached turbulent flows in an open channel. A backward facing step was used to induce flow separation. The rough surfaces comprised wire mesh grit-80 and sand grains of average diameter 1.5 mm. In each experiment, the Reynolds number based on the step height and freestream velocity of approach flow was fixed at 3240 and the Reynolds number based on the approach flow depth and freestream velocity was kept constant at 25130. Particle image velocimetry (PIV) technique was used to measure the flow velocity. The results showed that roughness effects on the mean and turbulent quantities are evident only in the recovery region. Moreover, roughness effects on the flow dynamics are dependent on the specific roughness element.

ACKNOWLEDGEMENT

I would like to express my sincere gratitude to my academic advisor, Dr. M. F. Tachie for his invaluable support throughout the programme. The understanding and encouragement from my dear husband, Yaw Owiredu Mante was a tremendous driving force for me from the start to the completion of my programme.

I am very grateful for the financial support provided by the Province of Manitoba (Manitoba Graduate Scholarship) and the University of Manitoba (University of Manitoba Graduate Fellowship and other awards).

I would like to express my appreciation for the training and technical support received from Dr. M. Agelinchaab, Godwin F. Tay, Paul Krueger and Kim Majury. The encouragement and support from my parents, Mr. and Mrs. Ampadu-Mintah and my siblings, Yaa Asantewaa, Afua Kesewaa, and Nana Yaw Asiedu are greatly appreciated. Last but not least, my sincere thanks go to all my friends especially, Terry Bruneau and family, Rev. Matthew Brough, Baafour Nyantekyi-Kwakye, Kwadwo Owusu Poku, Enoch A-Iyeh and Ebenezer E. Essel for their support and advice.

TABLE OF CONTENTS

ABSTRACT.....	i
ACKNOWLEDGEMENT.....	ii
TABLE OF CONTENTS.....	iii
LIST OF FIGURES.....	vi
LIST OF TABLES.....	x
NOMENCLATURE.....	xi
CHAPTER 1: INTRODUCTION.....	1
1.1 Motivation for research.....	1
1.2 Characteristics of various regions of separated and reattached turbulent flows.....	3
1.2.1 Upstream region.....	3
1.2.2 Separated region.....	4
1.2.3 Reattachment region.....	5
1.2.4 Recovery region.....	6
1.3 Problem statement.....	6
1.4 Specific objective and scope of research.....	7
CHAPTER 2: LITERATURE REVIEW.....	8
2.1 The boundary layer concept.....	8
2.2 Overview of canonical near wall turbulent flows.....	10
2.3 Classical open channel turbulent flows and rough wall turbulent boundary layer.....	12
2.3.1 Open channel turbulent flow.....	12
2.3.2 Rough wall turbulent boundary layer.....	13
2.4 Separated and reattached turbulent flows.....	14

2.4.1	Upstream region.....	16
2.4.2	Separated, reattachment and recovery regions.....	18
2.5	Summary of previous studies on separated and reattached turbulent flows	23
CHAPTER 3: EXPERIMENTAL SETUP AND MEASUREMENT		
	PROCEDURE.....	24
3.1	Experimental setup.....	24
3.2	The water tunnel facility.....	25
3.3	Test section.....	25
3.3.1	Roughness elements.....	27
3.4	Measurement procedure.....	28
3.4.1	Working principle of PIV.....	29
3.4.1.1	Seeding particles.....	30
3.4.1.2	Light source.....	31
3.4.1.3	Recording medium.....	31
3.4.2	PIV measurement procedure in present study.....	32
3.5	Test conditions.....	33
3.6	Convergence test.....	34
3.7	Measurement uncertainty.....	36
CHAPTER 4: RESULTS AND DISCUSSION.....		
4.1	Flow characteristics in the upstream region.....	37
4.2	Roughness effects in the separated and the reattachment regions.....	41
4.2.1	Mean flow characteristics.....	41
4.2.1.1	Contour of streamwise mean velocity and mean streamlines.....	41
4.2.1.2	Growth of separated shear layer.....	43

4.2.1.3	Mean velocity profiles.....	46
4.2.2	Reynolds stresses.....	48
4.2.3	Turbulence kinetic energy.....	52
4.2.4	Reynolds stress ratios.....	53
4.2.5	Turbulence energy production.....	55
4.2.6	Triple velocity correlation.....	57
4.3	Flow characteristics in the recovery region.....	59
4.3.1	Roughness effects on mean and turbulent statistics in the recovery region.....	60
4.3.1.1	Streamwise mean velocity.....	60
4.3.1.2	Reynolds stresses.....	61
4.3.1.3	Turbulence kinetic energy.....	63
4.3.1.4	Reynolds stress ratios.....	63
4.3.1.5	Triple velocity correlation.....	65
4.4	Roughness effects on the flow recovery process.....	66
4.5	Two point correlation analysis.....	68
CHAPTER 5: CONCLUSIONS AND RECOMMENDATIONS FOR FUTURE WORK.....		73
5.1	Conclusions.....	73
5.2	Recommendations for future work.....	74
REFERENCES.....		75

LIST OF FIGURES

Figure 1.1	Schematic of geometries for studying separated and reattached turbulent flows (h is the geometric height).....	2
Figure 1.2	Schematic of the various regions of flow over a backward facing step and the mean velocity profiles in the regions (U_e is the approach freestream velocity; x is the streamwise distance, y is the wall normal distance).....	3
Figure 2.1	Schematic of the various regions of a boundary layer.....	9
Figure 3.1	Experimental setup in the laboratory.....	24
Figure 3.2	Schematic of side view of (a) test section with planes of measurement ($P0 - P4$), (b) removable test surface (smooth), (c) removal test surface (rough). D is the water depth and h is the BFS height (<i>not drawn to scale: units in mm</i>).....	26
Figure 3.3	Roughness elements used to study surface roughness effects: (a) sand grain (b) wire mesh grit-80.....	28
Figure 3.4	Schematic of a typical setup of a PIV system.....	29
Figure 3.5	Profiles of mean and turbulent quantities obtained in the separated region ($x^* = 0.5$) and the recovery region ($x^* = 7$) using $N = 1000$ (\square), 3000 (\circ), 5000 (Δ): (a) U/U_e (b) u^2/U_e^2 (c) v^2/U_e^2 (d) $-uv/U_e^2$ (e) u^3/U_e^3 (f) v^3/U_e^3	35
Figure 4.1	Mean velocity profiles (a) in outer coordinates, (b) inner coordinates. The law of the wall (dotted line) and logarithmic law with $\kappa = 0.41$ and $B = 5.0$ (solid line) are shown for comparison.....	38

Figure 4.2	Turbulence intensities and Reynolds shear stress in (a) inner coordinates (b) outer coordinates.....	38
Figure 4.3	Distribution of mean streamwise velocity with mean streamlines in the separated and reattachment regions for (a) <i>SM</i> and (b) <i>WM</i>	42
Figure 4.4	Distribution of (a) maximum velocity difference, (b) maximum slope, (c) growth rate of vorticity thickness in the separated and the reattachment regions. Symbols: \square <i>SM</i> Δ <i>WM</i> \bullet <i>SG</i>	45
Figure 4.5	Distribution of local freestream velocity in the separated and reattachment regions Symbols: Symbols: \square <i>SM</i> Δ <i>WM</i> \bullet <i>SG</i>	46
Figure 4.6	Mean velocity profiles (a) streamwise (b) wall normal in the separated and reattachment regions. Symbols: \square <i>SM</i> Δ <i>WM</i> \bullet <i>SG</i> ...	47
Figure 4.7	Reynolds stresses in the separated and reattachment regions: (a) u^2/U_e^2 (b) v^2/U_e^2 (c) $-uv/U_e^2$. Symbols: \square <i>SM</i> Δ <i>WM</i> \bullet <i>SG</i>	49
Figure 4.8	y -locations where peak values of (a) u^2/U_e^2 , (b) v^2/U_e^2 and (c) $-uv/U_e^2$ occur along the dividing streamline. Symbols: \square <i>SM</i> Δ <i>WM</i> \bullet <i>SG</i>	51
Figure 4.9	Turbulent kinetic energy in the separated and reattachment regions. Symbols: \square <i>SM</i> Δ <i>WM</i> \bullet <i>SG</i>	53
Figure 4.10	Distribution of (a) v^2/u^2 and (b) $-uv/2k$ at selected streamwise locations in the separated and reattachment regions. Symbols: \square <i>SM</i> Δ <i>WM</i> \bullet <i>SG</i>	54
Figure 4.11	Turbulence production at various streamwise locations in the separated and reattachment regions. Symbols: \square <i>SM</i> Δ <i>WM</i> \bullet <i>SG</i> ...	56
Figure 4.12	Triple velocity correlation: (a) streamwise flux (b) wall normal	

	flux at various streamwise locations in the separated and reattachment regions. Symbols: $\square SM \triangle WM \bullet SG$	58
Figure 4.13	(a) Local freestream streamwise mean velocity (b) local boundary layer thickness at selected streamwise locations in the recovery region. Symbols: $\square SM \bullet SG$	60
Figure 4.14	Profiles of streamwise mean velocity in the recovery region. Symbols: $\square SM \bullet SG$	61
Figure 4.15	Profiles of Reynolds stresses in the recovery region: (a) u^2/U_e^2 (b) v^2/U_e^2 (c) $-uv/U_e^2$. Symbols: $\square SM \bullet SG$	62
Figure 4.16	Profiles of turbulence kinetic energy in the recovery region. Symbols: $\square SM \bullet SG$	63
Figure 4.17	Reynolds stress ratios in the recovery region; (a) v^2/u^2 (b) $-uv/2k$. Symbols: $\square SM \bullet SG$	64
Figure 4.18	Triple velocity correlation in the recovery region (a) streamwise flux (b) wall normal flux. Symbols: $\square SM \bullet SG$	65
Figure 4.19	Distribution of streamwise mean velocity (a) SM (b) SG ; distribution of streamwise Reynolds normal stress (c) SM and (d) SG	67
Figure 4.20	Distribution of streamwise Reynolds normal stress (a) SM (b) SG ; distribution of Reynolds shear stress (a) SM and (b) SG	68
Figure 4.21	Contours of R_{uu} at $x'' = 11$: centered at $y/\delta = 0.2$ (a) SM and (b) SG ; centered at $y/\delta = 0.6$ (c) SM and (d) SG ; outermost contour $R_{uu} = 0.5$, contour spacing = 0.1.....	69
Figure 4.22	Contours of R_{vv} at $x'' = 11$: centered at $y/\delta = 0.2$ (a) SM and (b) SG ; centered at $y/\delta = 0.6$ (c) SM and (d) SG ; outermost contour	

	$R_{vv} = 0.5$, contour spacing = 0.1.....	70
Figure 4.23	Extent of $R_{uu} = 0.5$ contour as a function of y/δ at $x'' = 2$ and 11: (a) streamwise extent (b) wall normal extent.....	71
Figure 4.24	Extent of $R_{vv} = 0.5$ contour as a function of y/δ at $x'' = 2$ and 11: (a) streamwise extent (b) wall normal extent.....	71

LIST OF TABLES

Table 2.1	Summary of prior studies on separated and reattached turbulent flows.....	15
-----------	---	----

NOMENCLATURE

English

B	Additive constant in logarithmic law
C_f	Skin friction coefficient
C_p	Pressure coefficient
d_{image}	Particle image diameter
d_p	Particle diameter
D	Water depth
$f\#$	f-number of the lens
F	Flatness factor
Fr	Froude number
g	Acceleration due to gravity
G	Clouser shape factor
h	step height
H	Shape factor
k	Turbulence kinetic energy
k_s	Equivalent sand grain roughness
l_m	Mixing length
Lx_{uu}	Streamwise extent of R_{uu}
Ly_{uu}	Wall normal extent of R_{uu}
Lx_{vv}	Streamwise extent of R_{vv}
Ly_{vv}	Wall normal extent of R_{vv}
P_k	Production of turbulent kinetic energy
Re_D	Reynolds number based on water depth and freestream velocity

Re_{θ}	Reynolds number based on momentum thickness and freestream velocity
Re_h	Reynolds number based on step height and freestream velocity
R_{uu}	Streamwise correlation coefficient
R_{vv}	Wall normal correlation coefficient
S	Skewness factor
u	Streamwise turbulence intensity
u^2	Streamwise Reynolds normal stress
U	Mean streamwise velocity
U_e	Local freestream velocity
U_o	Approach freestream velocity
U_{τ}	Friction velocity
ΔU	Maximum velocity difference
$-uv$	Reynolds shear stress
v	Wall-normal turbulence intensity
v^2	Wall normal Reynolds normal stress
v_s	Settling velocity
v_i	Velocity for an interrogation area
V	Mean wall normal velocity
w^2	Spanwise Reynolds normal stress
x	Streamwise distance
x'	Streamwise distance beyond reattachment
x_r	Reattachment length
y	Wall-normal distance
x^*	Streamwise distance normalized with reattachment length

$u^3, u^2v, uv^2,$ Triple correlations of fluctuating velocity components
 v^3, uvw^2, u^2w, w^3

Greek

δ	Boundary layer thickness
δ^*	Displacement thickness
δ^+	Reynolds number based on boundary layer thickness and friction velocity
δ_ω	Vorticity thickness
Δs	Local displacement vector
Δt	Laser time delay
ΔU	Maximum velocity difference
ΔU^+_{\max}	Maximum deviation from the log law line
ε	Turbulent dissipation rate
λ	Wave length
κ	von Kármán constant
ν	Kinematic viscosity
Π	Coles wake parameter
ρ_p	Particle density
ρ_f	Fluid density
τ_r	Particle response time
τ_w	Wall shear stress
θ	Momentum thickness

Superscript

- (+) Normalization with inner scales
- (*) Normalization with reattachment length with reference to the trailing edge of the step
- (") Normalization with reattachment length with reference to the reattachment point

Acronyms

BFS	Backward facing step
CCD	Charged coupled device
DNS	Direct numerical simulation
LDV	Laser Doppler anemometry
LES	Large eddy simulation
Nd: YAG	Neodymium: Yttrium Aluminum Garnet
PIV	Particle image velocimetry
PTV	Particle tracking velocimetry
ZPG	Zero pressure gradient

CHAPTER 1

INTRODUCTION

1.1 Motivation for research

Separated and reattached turbulent flows occur in several environmental and engineering fluid flow applications. Some of these applications are drainage systems, pipe systems, diffusers and atmospheric flows around hills. Flow separation usually results in increased mixing, and may also have significant impact on structural vibration and noise as well as drag, heat and momentum transport. Separated and reattached turbulent flows have been studied extensively by the turbulence research community over the past four decades in view of their diverse practical applications and potential impacts on turbulent transport phenomena. These studies were performed using both experimental techniques such as hotwire anemometry, laser Doppler velocimetry (LDV) and particle image velocimetry (PIV) (Adams and Johnston, 1988; Tachie *et al.*, 2001; Agelinchaab and Tachie, 2008) and numerical techniques such as direct numerical simulation (DNS) and large eddy simulation (LES) (Spalart, 1988; Barri1, 2010). The overarching objective in these studies was to better understand the mean and turbulence characteristics of the flow.

Configurations such as backward facing step (BFS), forward facing step, rib, fence, splitter plate and blunt plate have been used in the past to study separated and reattached turbulent flows. Schematic of these configurations is shown in Figure 1.1. Among these geometries, the BFS is the most extensively studied configuration perhaps due to its geometric simplicity. As can be seen in Figure 1.1, most of these geometries (for example, forward facing step, rib and fence) have more than one separating point, separated region and reattachment region whereas the flows over

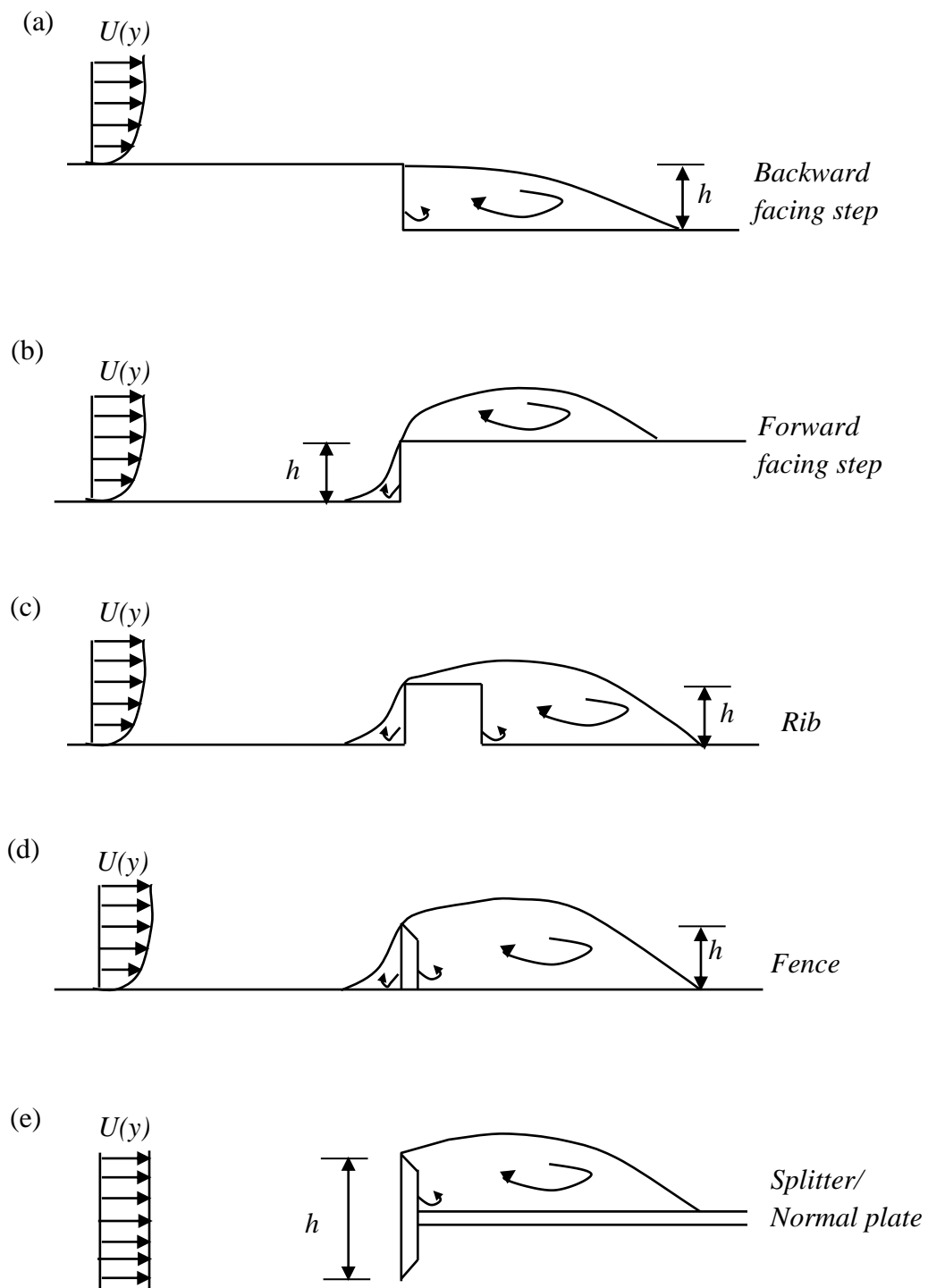


Figure 1.1: Schematic of geometries for studying separated and reattached turbulent flows (h is the geometric height)

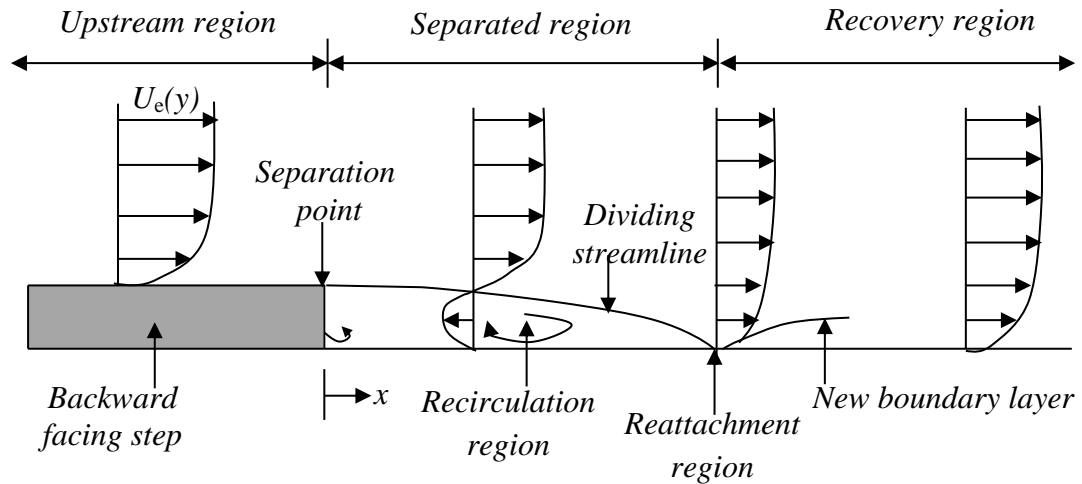


Figure 1.2: Schematic of the various regions of flow over a backward facing step and the mean velocity profiles in the regions (U_e is the approach freestream velocity; x is the streamwise distance, y is the wall normal distance)

BFS has a separation point fixed to the trailing edge of the step and has one separated region and one reattachment region. Irrespective of the geometry used to induce flow separation, the flow field can be categorised into an upstream region, a separated region (separated shear layer and recirculation region), a reattachment region and a recovery region. A schematic of these regions for flow over a backward facing step is shown in Figure 1.2. The flow characteristics of the various regions are presented in the following section.

1.2 Characteristics of various regions of separated and reattached turbulent flows

1.2.1 Upstream region

The upstream region corresponds to the region prior to separation, where the approach boundary layer develops. The characteristics of the approach flow have significant effects on the dynamics of separated and reattached turbulent flows. In this region, prior studies (Kasagi and Matsunaga, 1995; Piiro *et al.*, 2003) have shown that the

flow characteristics are similar to that of canonical near wall turbulent flow. Zero pressure gradient turbulent boundary layer (ZPG), fully developed pipe flow and channel flow are often referred to as canonical near wall flows. An overview of canonical near wall turbulent flow is provided in section 2.2.

1.2.2 Separated region

The approach boundary layer separates from the wall due to the presence of an obstacle or a change in surface geometry. After separation, the boundary layer is disrupted and there is a formation of a thin shear layer. The separated shear layer curves downward in the reattachment region and impinges on the wall. The separated shear layer is subjected to the effects of an adverse pressure gradient which is responsible for the first half of the shear layer being unaffected by the presence of the wall, thereby behaving like a free shear layer. Towards the reattachment region in the second half of the shear layer, there is a strong interaction between the shear layer and the wall (Adams and Johnston, 1988; Simpson, 1989). The turbulence levels are more intense in the separated shear layer than in the other regions of the flow. For example, the peak value of the streamwise turbulence intensity, wall normal turbulence intensity and the Reynolds shear stress reach their maximum of about 20%, 15% and 14% of the approach free stream velocity respectively (Kasagi and Matsunaga, 1995; Kostas *et al.*, 2002; Shah, 2008).

Beneath the separated shear layer is the recirculating flow region. This region of the flow is a result of the shear layer fluid being deflected upstream as it impinges onto the wall. This region is characterized with both negative and positive mean velocities with substantial negative values of streamwise mean velocity (U) being reported. For example, for flow over BFS, the maximum negative streamwise mean velocity has

been observed to fall within a range of 10% to 20% of the freestream streamwise mean velocity (U_e) (Eaton and Johnston, 1981; Kasagi and Matsunaga, 1995; Jovic, 1996). Djilali and Gartshore (1991) observed a maximum negative velocity of about $0.30U_e$ for a bluff plate. For the wall normal velocity (V), Kasagi and Matsunaga (1995) observed a maximum value of $0.08U_e$ for separated and reattached turbulent flows over a BFS. Agelinchaab and Tachie (2008) reported a maximum value of $V = 0.08U_e$ for separated and reattached turbulent flow over a square rib in an open channel while $0.25U_e$ was observed by Shah (2008) in separated and reattached turbulent flow over ribs. It has been noted that the streamwise mean velocity (U) and the wall normal mean velocity (V) in this region are comparable. This observation implies that the usual boundary layer approximation that the wall normal mean velocity is negligibly small compared to the streamwise mean velocity is not valid in the separated region (Agelinchaab and Tachie, 2008).

1.2.3 Reattachment region

Given some distance, the separated shear layer reattaches onto the wall and then a new boundary layer develops. The location where the flow reattaches and the characteristics of the flow in the reattachment region play a significant role in the development of the recirculation region and then the initiation of the flow recovery process. The reattachment region is a sensitive region and is influenced by several factors such as the geometry for inducing separation, Reynolds number, perturbation strength (which is the ratio of the boundary layer thickness (δ) to step height (h)), the state of the boundary layer at the separation point, expansion ratio (which is the ratio of step downstream height to step upstream height), freestream turbulence and surface roughness (Simpson, 1989; Castro and Epik, 1998). These parameters have resulted in a wide range of values for the reattachment length. For flows over BFS, for example,

values of $4h$ to $8h$ have been reported (Nakagawa and Nezu, 1987; Adams and Johnston, 1988; Kasagi and Matsunaga, 1995). Agelinchaab and Tachie (2008) observed a reattachment length of $8.5h$, $6.7h$ and $10.1h$, respectively, for flows over square, semicircular and rectangular prisms in an open channel whereas for flows over a forward facing step, reattachment length of $1.1h$ to $4h$ was observed by Sherry *et al.* (2009).

1.2.4 Recovery region

A new boundary layer develops after the reattachment of the separated shear layer. Prior studies (Castro and Epik, 1998; Agelinchaab and Tachie, 2008) have demonstrated that the recovery of the flow is extremely slow and that the recovery of the outer boundary layer is far slower than the inner boundary layer. This is because the outer layer carries large eddy structures from the separated shear layer which takes several step heights to decay. The recovery process may depend on factors such as the type of geometry used for inducing flow separation and freestream turbulence.

1.3 Problem statement

Prior studies have significantly improved our understanding of separated and reattached turbulent flows. However, most of these studies focused on separated and reattached turbulent flows over a smooth surface with zero pressure gradient (ZPG). Meanwhile, many environmental and technological applications have free surface boundary conditions. In these applications, surface roughness is also a defining feature. For example, surface roughness may emanate from biomass accumulation, debris deposition, corrosion, sedimentation, cavitation effect, erosion effect and manufacturing defects. From prior studies on rough wall turbulent boundary layer (Tachie *et al.*, 2003; Schultz and Flack, 2007; Tay, 2009), it was demonstrated that

surface roughness increases drag and may also have significant impact on turbulent transport phenomena. There is, therefore, a need to understand the effects of surface roughness on the dynamics of separated and reattached turbulent flows in open channels.

1.4 Specific objective and scope of research

The specific objective of this research is to study the effect of surface roughness on the dynamics of turbulent flow downstream of a BFS in an open channel. This objective is achieved by conducting an experimental research to study the velocity field in the various flow regions using a particle image velocimetry (PIV) technique. The characteristics of the flow are studied by analyzing the mean velocities, Reynolds stresses, Reynolds stress ratios, triple velocity correlations, turbulent kinetic energy and the production term of the turbulence kinetic energy transport equation. A two point spatial correlation function is used to examine the statistical features of the coherent structures. This research contributes to the understanding of the nature of separated and reattached turbulent flow over smooth and rough surfaces in an open channel. It also provides benchmark datasets for validating numerical results and will facilitate the development of more accurate turbulence models for practical flow applications.

CHAPTER 2

LITERATURE REVIEW

This chapter presents a review of previous studies on separated and reattached turbulent flows with ZPG and open channel. In order to facilitate our understanding of the complex nature of separated and reattached turbulent flows, an overview of boundary layer concept and the characteristics of near wall turbulent flows over smooth and rough walls are presented before the review of the previous studies on separated and reattached turbulent flows.

2.1 The boundary layer concept

The boundary layer concept was introduced by Ludwig Prandtl, a German aerodynamicist in 1904. This concept was introduced to bridge the difficulty in the analysis of real fluid flows in engineering applications as opposed to ideal flows, where no drag is experienced. The boundary layer is defined as part of the flow near the wall where viscous effects are dominant. The viscous effects retard the fluid motion which results in slow moving particles near the wall and they in turn retard the motion of the adjacent fluid particles. In the region outside of the boundary layer, the effect of viscosity is negligible and the fluid may be treated as inviscid.

Boundary layer may be either laminar or turbulent depending on the value of the Reynolds number. At relatively low Reynolds numbers, the boundary layer is laminar, and in this case, the velocity gradient is small and the wall shear stress is low. At relatively high Reynolds numbers, the boundary layer is said to be turbulent. For a turbulent boundary layer, the mean velocity profile changes rapidly in the vicinity of the wall so that the velocity gradient close to the wall and hence the wall shear stress

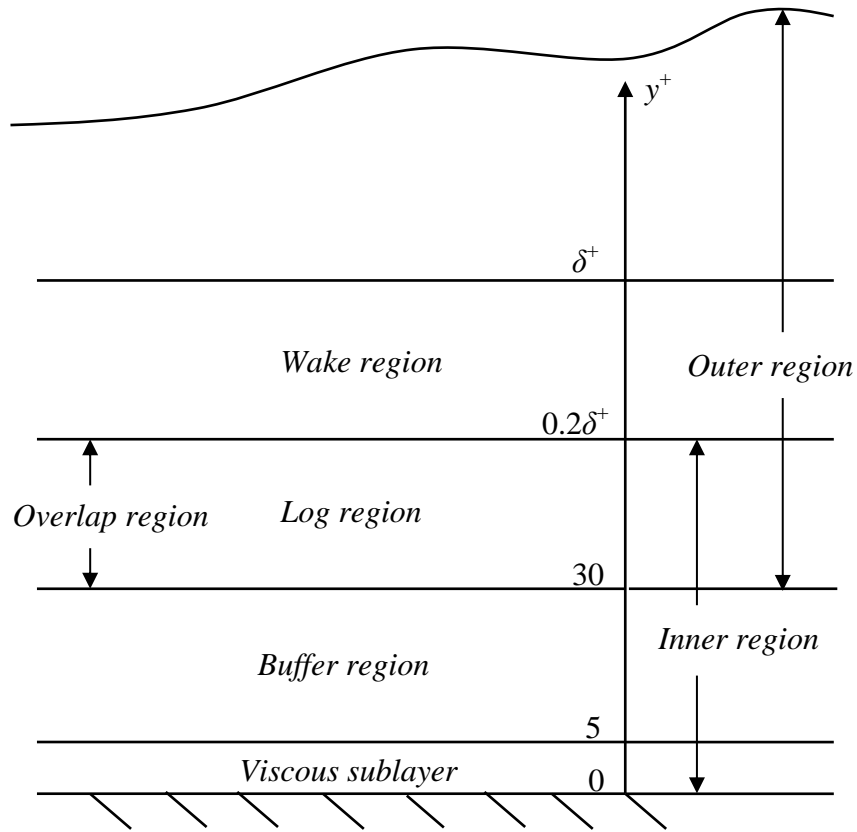


Figure 2.1: Schematic of the various regions of a boundary layer

are substantially higher than for a laminar boundary layer. In a turbulent boundary layer, the flow field is also much more complicated than in a laminar boundary layer. For example, unlike laminar flows, the velocity field of turbulent flows is not repeatable in either the whole or part of the flow domain.

A typical turbulent boundary layer can be divided into two distinct layers; namely the inner region and the outer region. In the inner region, viscosity plays an important role on the dynamics of the flow, while the outer region of the boundary layer is dominated by inertial effects. In the limit, as the Reynolds number approaches infinity, there exists an overlap region over which the two layers interact. The extent of the various regions in terms of wall variables is shown in Figure 2.1. In the figure, $\delta^+ = \delta U_\tau / \nu$, and $y^+ = y U_\tau / \nu$, where y is the wall normal distance from the wall, δ is the

boundary layer thickness which is defined as the wall normal distance at which the local mean streamwise velocity (U) is 99% of the freestream streamwise mean velocity (U_e), U_τ is the friction velocity which is related to the wall shear stress (τ_w) and the density of the fluid (ρ) as $\sqrt{(\tau_w/\rho)}$, and ν is the kinematic viscosity of the fluid. As illustrated in Figure 2.1, the inner region comprises the viscous sublayer, the buffer region and the overlap region. The velocity profile varies linearly with distance from the wall (that is $U^+ = y^+$, where $U^+ = U/U_\tau$) in the viscous sublayer, which may extend from the wall to $y^+ = 5$. The buffer region extends from $y^+ = 5$ to 30 while the outer region of the boundary layer extends from $y^+ = 30$ to δ^+ . The overlap region extends from $y^+ = 30$ to $0.2 \delta^+$.

2.2 Overview of canonical near wall turbulent flows

To a great extent, the main success of turbulent boundary layer analysis is dependent on canonical near wall turbulent flows due to their simplicity with respect to both physics and geometry. These flows form the basis for the understanding of the more complex near wall flows encountered in engineering applications. In canonical near wall turbulent flows, most of the studies were done to study Reynolds number effects on the flow characteristics. In canonical near wall turbulent flow research, there are variations in the Reynolds numbers used. Some of these Reynolds numbers are Reynolds number based on boundary layer momentum thickness $Re_\theta (= \theta U_e/\nu)$, Reynolds number based on half channel height $Re_h (= hU_e/\nu)$, and Reynolds number based on boundary layer thickness and friction velocity $\delta^+ (= \delta U_\tau/\nu)$.

It should be remarked that in the laboratory, the flows studied are of Reynolds numbers far less than that encountered in most practical flow applications. This implies that the data obtained in the laboratory would have to be extrapolated to the

high Reynolds number flows encountered in practical flow applications. To be able to extrapolate the low Reynolds number flows to the high Reynolds number flows, a proper scaling is required to non-dimensionalize the quantities that are used to characterize the flow. According to similarity law, when a proper length and velocity scales are used for non-dimensionalizing the quantities, irrespective of the facilities used for the study at different Reynolds numbers, the quantities will collapse to a single profile at least in the inner region (Gad-el-Hak and Bandyopadhyay, 1994). This has resulted in many attempts in finding the correct velocity and length scales for the quantities used to characterize canonical near wall turbulent flows. According to classical theories of turbulent flow, the inner region of canonical near wall turbulent flows is scaled on friction velocity (U_τ) and viscous length (ν/U_τ) as the velocity scale and length scale respectively whereas the outer layer is presumed to scale on the outer scales which are the freestream velocity (U_e) and the boundary layer thickness (δ).

The classical logarithmic law ($U^+ = \kappa^{-1} \ln y^+ + B$, where κ and B are logarithmic law constants) has been extensively used to describe the mean streamwise velocity in the overlap region. It was observed in previous studies that increasing Reynolds number increased the extent over which the data collapses on the logarithmic law profile. The outer layer of the boundary layer in inner scale is usually examined from the maximum deviation of the data from the logarithmic law, ΔU_{\max}^+ which is related to the strength of the wake as $\Delta U_{\max}^+ = 2\Pi/\kappa$ (where Π is the wake parameter). Previous studies have demonstrated that Π increases with Reynolds number and asymptotes to 0.55 at high Reynolds number ($Re_\theta \geq 6000$) (Coles, 1956; Fernholz and Finley, 1996).

Profiles of the mean velocity in outer scale become more uniform with corresponding decrease in both the shape factor ($H = \delta^*/\theta$, where δ^* is the mass displacement

thickness, θ is momentum thickness associated with the boundary layer) and the skin friction coefficient as Reynolds number increases. This is attributed to the diminishing effects of viscosity as Reynolds number increases and allowing inertia effects to dominate (Gad-el-Hak and Bandyopadhyay, 1994).

2.3 Classical open channel turbulent flow and rough wall turbulent boundary layer

An overview of classical open channel turbulent flow (hereafter referred to as open channel turbulent flow) and rough wall turbulent boundary layer is given in this section. This is done to establish that the characteristics of simple canonical near wall turbulent flows are modified by free surface, and surface roughness and therefore should not be ignored in a complex flow like separated and reattached turbulent flow.

2.3.1 Open channel turbulent flow

The understanding of turbulent flows in open channel is very important since many fluid engineering applications such as drainage systems, irrigation canals and water and waste water treatment systems have free surface boundary conditions. In open channel flows, Froude number ($Fr = U/\sqrt{gD}$, where g is the gravitational constant $= 9.81 \text{ m/s}^2$, and D is the water depth) is a vital dimensionless parameter which is used to classify the flow into a subcritical regime ($Fr < 1$), a critical regime ($Fr = 1$) and a supercritical regime ($Fr > 1$). It should be noted that the regime of an open channel flow may affect the extent of the disturbance of the free surface. Subcritical flows have gentle wavy surface whereas supercritical flows are more rapid with highly disturbed free surface.

Similar to canonical near wall turbulent flows, open channel turbulent boundary layer can be divided into two regions: an inner region and an outer region. The velocity and

length scales used in canonical near wall turbulent flows have been adopted in the analysis of open channel flows. It has been demonstrated in previous studies of open channel turbulent flows (Nezu and Rodi, 1986; Tachie *et al.*, 2003; Afzal *et al.*, 2009) that the characteristics of the mean streamwise velocity in the inner region are similar to those observed in canonical near wall turbulent flows. Also, previous studies have demonstrated that the magnitude of Reynolds stresses in open channel turbulent flow compares reasonably well with that observed for canonical near wall turbulent flow (Nezu and Rodi, 1986). In the outer region, however, the presence of the free surface, characterized by high freestream turbulence, causes considerable changes in the boundary layer. For instance, it causes an increase in the magnitude of skin friction coefficient and decreases the wake region compared to corresponding values for canonical near wall turbulent flows at similar Reynolds numbers (Tachie *et al.*, 2003; Afzal *et al.*, 2009).

2.3.2 Rough wall turbulent boundary layer

As noted earlier in section 1.3, surface roughness is a defining feature in real fluid flow applications. Surface roughness may emanate from biomass accumulation, debris deposition, corrosion, sedimentation, manufacturing defects and effects from cavitation and erosion. Different materials such as sand grains, uniform spheres and wire mesh have been used in the past to generate different degrees of roughness in the laboratory. Based on Nikuradse's equivalent sand grain roughness height (k_s) in inner variable, k_s^+ (Nikuradse, 1933), Schlichting (1979) proposed that a surface can be classified into one of the following three different roughness regimes: hydrodynamically smooth for $k_s^+ < 5$, transitionally rough for the range $5 < k_s^+ < 70$ and fully rough for $k_s^+ > 70$. This implies that for a hydrodynamically smooth surface, the effective roughness height is smaller than the viscous sublayer. In transitionally

rough regime the effect of roughness is felt within the buffer layer. For fully rough regime, the roughness effect may extend well into the overlap and outer regions.

Previous studies (Krogstad and Antonia, 1999; Tachie *et al.*, 2003; Djenidi *et al.*, 2008) have demonstrated that the mean velocity profile in inner coordinates shows roughness effects by producing a downward shift below that of a smooth wall mean velocity profile and the shift increases with increasing k_s^+ . In outer coordinates, the mean velocity profile for rough wall is less uniform than that over a smooth wall at a similar Reynolds number. As a result, roughness increases the magnitude of the shape factor compared to a smooth wall. Also, in contrast to a smooth wall boundary layer, at similar Reynolds number, the skin friction coefficient increases with increasing roughness. Surface roughness also causes a significant increase in the magnitude of the higher order turbulent statistics comparison to smooth wall boundary layer at similar Reynolds number (Tachie *et al.*, 2003; Schultz and Flack, 2007; Tay, 2009).

2.4 Separated and reattached turbulent flows

It should be acknowledged that many turbulent flows encountered in engineering applications are different, and relatively more complex than the well-studied turbulent boundary layers. An example of these complex turbulent flows is separated and reattached turbulent flow, which is the focus of this present study. The relative complex nature of separated and reattached turbulent flows makes them acute sensitive test cases for assessing turbulent models for engineering applications. Consequently, several studies have been conducted in the past using geometries such as backward facing step (BFS), forward facing step, blunt plate, fence, and ribs to induce flow separation. These configurations were schematically shown in Figure 1.1.

Table 2.1: Summary of prior studies on separated and reattached turbulent flows

Author	Geometry	Technique	Re_h	Quantities
Tachie <i>et al.</i> (2003)	Forward facing step	LDV	960-1890	$U, x_r, u, C_f, H, G,$
Piirto <i>et al.</i> (2003)	Backward facing step	PIV	15000	$U, x_r, u, v, uv,$ <i>Budget terms</i>
Castro and Epik (1998)	Blunt Plate	Hot-wire	6500	$U, x_r, u^2, v^2, w^2, -$ $uv, u^3, u^2v, uv^2, v^3,$ $uw^2, u^2w, w^3, S_w, F_w$ <i>Budget terms</i>
Adams and Johnston (1988)	Backward facing step	Hotwire, Thermal tuft	8000-40000	x_r, C_f
Kasagi and Matsunaga (1995)	Backward facing step	PTV	5540	$U, x_r, u, v, w, -uv, u^3,$ $u^2v, uv^2, v^3, uw^2, u^2w,$ <i>Budget terms</i>
Le <i>et al.</i> (1997)	Backward facing step	DNS	5100	$U, x_r, C_f, u, v, uv,$ <i>Budget terms</i>
Piirto <i>et al.</i> (2003)	Backward facing step	PIV	15000	$U, x_r, u, v, uv,$ <i>Budget terms</i>
Agelinchaab and Tachie (2008)	Square, rectangular and semicircular prisms	PIV	1900	$U, x_r, \theta, C_f, H, G, u,$ $v, -uv, u^3, uv^2, u^2v, v^3,$ P_k, lm
Tachie <i>et al.</i> (2003)	Forward facing step	LDV	960-1890	$U, x_r, u, C_f, H, G,$
Nakagawa and Nezu (1987)	Backward facing step	LDV	8200-23400	$U, V, x_r, u, v, -uv, C_f,$ $\tau_w, C_p, \text{Budget terms}$
Song and Eaton (2002)	Contoured ramp	LDV	315000	U, u^2, v^2, uv, P_k
Kim and Chung (1994)	BFS	Split film sensor	26500	U, x_r, u^2, H

As indicated earlier in section 1.1, over the past four decades, significant amount of research has been dedicated to the understanding of separated and reattached turbulent flows. Some of these studies are summarized in Table 2.1. The information provided in Table 2.1 includes the geometry used to induce flow separation, the measurement techniques, Reynolds number based on step height and freestream or centerline velocity (Re_h) and the quantities used to analyze the characteristics of the flow. It should be noted that U and V are the mean velocities in the streamwise and wall normal directions respectively, u , v and w are the fluctuating components in the streamwise, wall normal and spanwise directions respectively, x_r is the reattachment length, C_f is the skin friction coefficient, C_p is the wall pressure coefficient, G is the Clauser parameter, H is the shape factor, θ is the momentum thickness, τ_w is the wall shear stress, k is the turbulent kinetic energy, P_k and ε are, respectively, the production and the dissipation rate of turbulent kinetic energy, l_m is the mixing length, S and F are respectively, the skewness and flatness factors. In the subsequent sections some of the observations made in the various regions of previous studies that informed the scope of the present study are presented. The observations are presented in two sections: the first section presents observations in the upstream region and the second section presents observations in the separated region, the reattachment region and the recovery region.

2.4.1 Upstream region

As already mentioned in section 1.2.1, the upstream region corresponds to the region prior to separation, where the approach boundary layer develops. Because the dynamics of the other regions are sensitive to the upstream conditions, significant efforts have been made in previous studies to document the characteristics of the approach flow. Also, analyzing the upstream region of the flow provides information

for the inlet boundary conditions for numerical studies of separated and reattached turbulent flows. Kasagi and Matsunaga (1995) carried out experiments to study ZPG flows over BFS. The Reynolds number based on step height and centerline velocity, Re_h of the flow was 5540 with an expansion ratio (ratio of step downstream height to step upstream height) of 1.5. The velocity field was measured with a particle tracking velocimetry (PTV) technique. It was demonstrated that the characteristics of the flow in the upstream region are similar to that observed in canonical near wall turbulent flows. For example, it was observed that the streamwise mean velocity followed the classical logarithmic law. With respect to the turbulence intensities, they observed a peak value of 2.8, 1.0 and 1.3 respectively for the streamwise, wall normal and spanwise turbulence intensities in inner coordinates which also compare reasonably well with that observed in canonical near wall turbulent flows. A similar observation was made by Piiro *et al.* (2003) in a study of ZPG flow over a BFS at three different values of Re_h (12000, 21000, and 55000) with an expansion ratio of 1.2. The velocity field was measured with a PIV.

Tachie *et al.* (2001) also reported velocity measurements in the upstream region of turbulent flows over a forward facing step in an open channel with an LDV at Re_h ranging from 960 to 1890. Similar to observations made by Kasagi and Matsunaga (1995) and Piiro *et al.* (2003), Tachie *et al.* (2001) observed that the characteristics of the mean streamwise velocity in the inner region of the boundary layer are similar to those observed in canonical near wall turbulent flows. In the outer region, however, a value of $II \leq 0.2$ was reported. These II values are less than a typical value of 0.55 observed in canonical near wall turbulent flows at high Reynolds numbers (Coles, 1956). This observation is consistent with other results obtained in open channel turbulent flows (Nezu and Rodi, 1986; Tachie *et al.*, 2003). Similar to

observation by Kasagi and Matsunaga (1995) and Piirto *et al.* (2003), Tachie *et al.* (2001) reported a peak value of 2.78 for streamwise turbulence intensity in inner coordinates.

2.4.2 Separated, reattachment and recovery regions

As mentioned earlier in section 1.1, turbulent flows over BFS is the most studied separated and reattached turbulent flow due to its geometric simplicity. One of the detailed studies on BFS flows is the experimental study of Kasagi and Matsunaga (1995). The Reynolds number based on step height and centerline velocity, Re_h was 5540 and the expansion ratio was 1.5. The velocity field was measured with a PTV. The reattachment length was determined using the forward fraction method which is the streamwise location where the time fraction of forward (streamwise) flow is equal to 0.5 toward the wall. It was observed that after the separation of the approach boundary layer at the trailing edge of the step, the mean flow reattached at $x/h = 6.51$. Beneath the separated shear layer, they observed primary recirculation and corner eddy behind the BFS. In the recirculation region, the maximum negative streamwise mean velocity observed was $0.2U_c$. The levels of turbulence intensities and Reynolds shear stress were much higher in the separated free shear layer than in the other regions of the flow. Maximum values of $0.2U_c$ for the streamwise turbulence intensity, $0.18U_c$ for both the wall normal and spanwise turbulence intensities and $0.013U_c^2$ for the Reynolds shear stress were observed. They also observed that turbulent diffusion plays a significant role in the transport of turbulence kinetic energy in the separated region and the early part of the recovery region. In the near wall region at $y/h < 0.15$, turbulence diffusion balances out dissipation of turbulence energy due to low turbulence production rate in the near wall region.

A thorough experimental investigation on the reattachment length of flows over a BFS was carried out by Adams and Johnston (1988). This study investigated the effects of perturbation strength, upstream boundary layer state and Reynolds number on turbulent flows over a BFS. The Re_h ranged from 8000 to 40000, the perturbation strength ranged from 0.005 to 1.7. The expansion ratio of the flow was fixed at 1.2. The velocity field of the flow was measured with a hotwire. The reattachment length was determined using the forward fraction method. They observed a reattachment length of approximately $6.5h$ for flows with fully turbulent upstream boundary layer condition. This shows that the reattachment length is independent of Reynolds number and perturbation strength if the upstream boundary layer state is fully turbulent. It should be noted that fully turbulent upstream boundary layer state in this study was defined based on the near-wall turbulence level and the appropriateness of the log-law fit for the mean velocity profile as in the case of canonical near wall turbulent flows. The reattachment length determined by Adams and Johnston (1988) is in good agreement with 6.51 observed by Kasagi and Matsunaga (1995).

Another detailed experimental research on turbulent flows over a BFS was performed by Nakagawa and Nezu (1987) to study Reynolds number effects on turbulent flows over a BFS in an open channel. The open channel flow was in the subcritical flow regime with Froude number ranging from 0.12 to 0.33. The Re_h studied ranged from 8200 to 23400, and the velocity field was measured with an LDV. The reattachment length of the mean flow was determined from the stream function method, that is, the streamwise location where the zero contour of the stream function ($\psi = \int_0^y U dy$) impinges on the wall. This study demonstrated that increasing the Reynolds number and the Froude number caused a reduction in the reattachment length from $6.3h$ and attained a constant value of about $5.0h$. The Reynolds number range in this study falls

within 8000 to 40000 studied by Adams and Johnston (1988) where they attained a constant value of about $6.5h$. The lower values of reattachment length in this study may be attributed to the free surface effects. Similar to observation made by Kasagi and Matsunaga (1995), the turbulence intensities and Reynolds shear stress attained their peak in the separated shear layer and then decayed rapidly after reattachment.

Ötügen (1991) carried out an experimental research to study expansion ratio effects on turbulent flows over BFS at Re_h of 16600 with expansion ratio ranging from 0.5 to 2.13. The velocity field was measured with an LDV. The reattachment length was measured using the forward fraction method. This study showed that there is an inverse relation between the expansion ratio and the reattachment length. That is, increasing the expansion ratio from 0.5 to 2.13 decreased reattachment length from $7h$ to $6h$. It was also demonstrated that increasing the expansion ratio increased the levels of the streamwise turbulence intensity. For expansion ratio of 2.13, the peak value observed for the streamwise turbulence intensity was $0.16U_e$ compared to $0.09U_e$ observed for expansion ratio of 0.5. This effect was more significant in the early stage of the separated shear layer, that is, at $x/h = 0.6$.

Le *et al.* (1997) studied turbulent flow over a BFS using a DNS approach at Re_h of 5100 with an expansion ratio of 1.20. A reattachment length of $6.28h$ was observed. In the separated shear layer, dissipation was observed to be about 40% of the production, which shows that the flow is not in energy equilibrium. This was attributed to the turbulence diffusion and mean flow convection being non-negligible. Similar to observation made by Kasagi and Matsunaga (1995), in the near wall region in the recirculation and the reattachment regions, turbulence diffusion balances dissipation.

Kim and Chung (1994) conducted experimental research to study surface roughness effects on turbulent flow downstream of a BFS. The roughness elements studied were d and k -types (where d -type of roughness is when the ratio of the roughness width to its height is less than one and vice-versa for the k - type). The Re_h was 26500 and the velocity field was measured with a split film sensor. The reattachment length was determined using the forward fraction method. The study showed that the k -type roughness increased the reattachment length from $5.86h$ to $6.06h$. They observed no significant effect of surface roughness on the distribution of streamwise mean velocity and the streamwise Reynolds normal stress in the separated and the reattachment regions.

Agelinchaab and Tachie (2008) carried out experiments to study the effects of geometries for inducing separation in an open channel at Re_h of 1900. The open channel flow was in the subcritical flow regime with $Fr = 0.34$. The geometries studied include semicircular, square and rectangular prisms. The velocity field of the flow was measured with a PIV. The reattachment length of the mean flow was determined as the location at which the dividing mean streamline impinges on the wall. This study demonstrated that the reattachment length varied with geometry. That is, reattachment length of $6.7h$, $8.5h$, and $10.1h$ was observed for the semicircular, square and rectangular prisms respectively. Similar to other studies, the turbulence intensities and Reynolds shear stress attained their maximum in the separated region but their magnitude showed geometry dependence. The study also demonstrated that the rate of turbulence production is low whereas turbulence diffusion is high in the near wall region in the separated and reattachment regions, which is consistent with observation made by Le *et al.* (1996) and Kasagi and Masunaga (1995). The study showed that the recovery of the flow is geometry dependent up to $x/h = 50$ beyond

reattachment. Subsequently ($x/h > 50$), the recovery of the flow did not show significant effects of the geometry although complete similarity with the upstream was not achieved.

Tachie *et al.* (2001) carried out experimental research to study the recovery region of turbulent flows over forward facing step in an open channel at Re_h ranging from 960 to 1890. The velocity field was measured with an LDV. This study showed that the streamwise mean velocity profiles attained similarity with the upstream profiles beyond $x/h = 50$. However, the collapse of the streamwise turbulence intensity on the upstream profile was not achieved even at $x/h = 100$ after the reattachment.

Castro and Epik (1998) carried out experimental research to study the effects of free stream turbulence on the recovery of turbulent flow over a blunt plate at Re_h of 6500. The freestream turbulence of the flow was 5% which is far higher than that in typical wind tunnel experiments. The velocity field of the flow was measured with a hotwire and the reattachment length was determined using a pulsed wire technique. This study showed that freestream turbulence reduces the size of the recirculation region by about 20% which should cause a significant reduction in the reattachment length. However, the flow condition was adjusted to ensure the same reattachment length for both the freestream turbulence and non-freestream turbulence. Hence a reattachment length of $7.7h$ was observed for both non-freestream turbulence and freestream turbulence. It was shown that at the reattachment point, freestream turbulence enhanced the levels of Reynolds stresses by over 150%. Further downstream, at $x/h = 154$, freestream turbulence has no significant effects on the turbulent quantities but the flow has not yet recovered.

2.5 Summary of previous studies on separated and reattached turbulent flows

The review of previous studies on separated and reattached turbulent flows showed that separated and reattached turbulent flows have been extensively studied using different geometries such as backward facing step, forward facing step, rib and blunt plate. Experimental and numerical approaches have been employed to reveal the salient features of the flows. Turbulent quantities up to the fourth order and budget terms have been reported. It was demonstrated that the upstream region has characteristics similar to canonical near wall turbulent flows. Turbulence levels are significantly higher in the separated shear layer than in the other regions of the flow. Energy equilibrium is not achieved in the separated region through to the early recovery region due to non-negligible turbulence diffusion and convection. The reattachment region is influenced by factors such as geometry used to induce flow separation, Reynolds number, perturbation strength, the state of the approach boundary layer, expansion ratio, freestream turbulence and surface roughness. After the reattachment of the separated shear layer, the flow recovery is a slow process and takes several step heights to recover due to large eddies being carried from the separated shear layer and takes several step heights to decay. The recovery process is influenced by factors such as geometry for inducing flow separation, upstream boundary conditions and freestream turbulence.

CHAPTER 3

EXPERIMENTAL SETUP AND MEASUREMENT PROCEDURE

This chapter presents the description of the experimental setup, test conditions, measurement procedure, convergence test and then the measurement uncertainty in the datasets.

3.1 Experimental setup

The experimental setup in the laboratory is as shown in Figure 3.1. The setup comprised a main water tunnel facility, a test section that was inserted into the main water tunnel and a PIV system. The subsequent sections provide detailed description of the various components of the setup.



Figure 3.1: Experimental setup in the laboratory

3.2 The water tunnel facility

The water tunnel was designed and constructed by Engineering Laboratory Design, Inc., Minnesota, USA. The water tunnel consists of flow settling chamber for flow conditioning, test section, pump, variable speed drive, piping, supporting framework and filtering station. The overall dimensions of the unit are: 5370 mm in length, 1435 mm in width and 1822 mm in height. The settling chamber is made up of perforated steel plates and honeycomb designed to ensure quality flow transition from high speed pipe velocities to low speed test section velocities, while reducing turbulence and providing flow uniformity. The test section is an open channel fabricated with Super Abrasion Resistant[®] (SAR) clear acrylic to facilitate optical access and flow visualization. The interior dimensions of the test section are 2500 mm long by 200 mm wide by 200 mm deep. A 25 hp transistor inverter type variable speed controller regulates the speed of the motor that drives the pump. A filter system is furnished as a means of removing contaminants from the system's water.

3.3 Test section

In order to achieve the test conditions for this study, a test section was manufactured and inserted into the test section of the main water tunnel. Figure 3.2(a) shows the schematic of side view of the open channel test section which was inserted into the main water tunnel to carry out the experiments. The wall of the test section was made of 6 ± 0.1 mm acrylic plate to facilitate optical access with dimensions 2500 mm long, 188 mm wide and 195 mm deep. The width and height of the test section are less than the main tunnel test section because of the wall thickness. The test section was supported in the main water tunnel by means of screws at the entrance and exit of the test section.

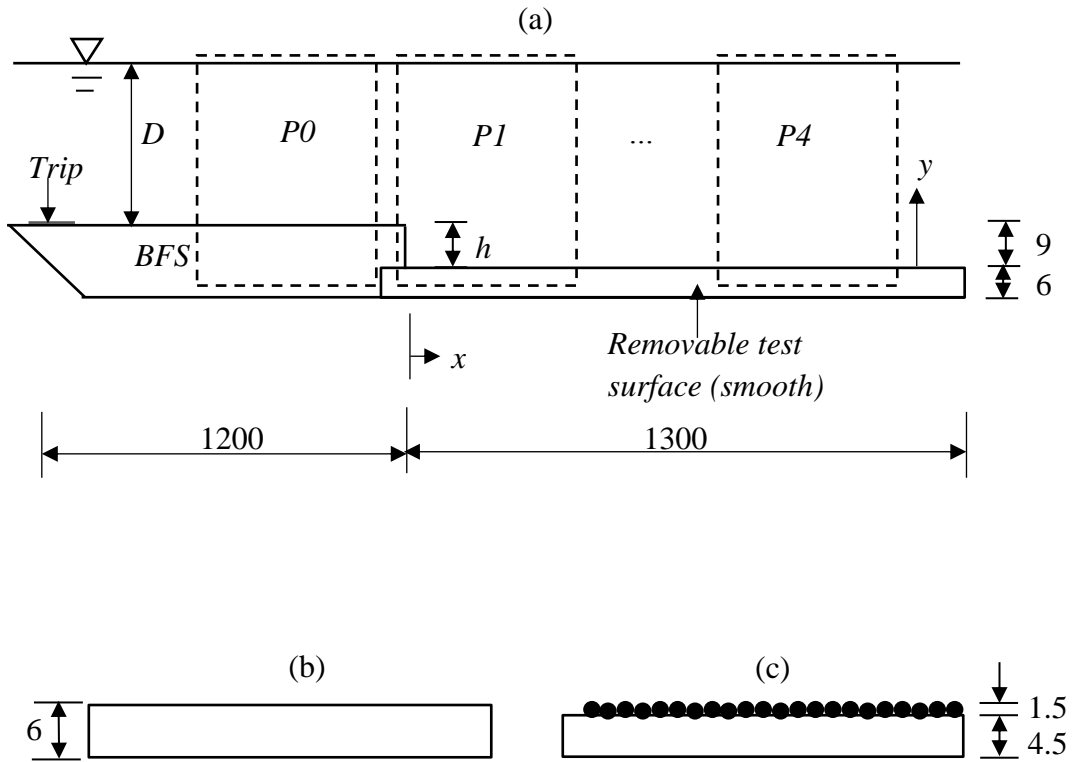


Figure 3.2: Schematic of side view of (a) test section with planes of measurement ($P0 - P4$), (b) removable test surface (smooth), (c) removal test surface (rough). D is the water depth and h is the BFS height (*not drawn to scale: units in mm*)

Figure 3.2(a) also shows the trip used to enhance the development of the turbulent boundary layer, the BFS used to induce flow separation, a removable test surface for studying the flow characteristics over smooth and rough surfaces, the planes of velocity measurement and the coordinate system adopted in the present study. The BFS was made of hydraulically smooth acrylic plate of thickness 9 ± 0.1 mm. The BFS spanned the entire width and the first 1200 mm of the test section. The height of the BFS was chosen in order to attain a two dimensional flow: the aspect ratio (ratio of channel width to step height) of the channel was determined to be 21, which is higher than 10 which is the threshold for establishing nominally two dimensional separated and reattached turbulent flows. The choice of the length of the BFS was based on ensuring a fully turbulent flow development of the approach flow before separation.

Figure 3.2 (b-c) shows the individual removable test surfaces to produce the smooth and rough surfaces downstream of the BFS. The smooth surface was made of 6 ± 0.1 mm thick acrylic plate. For the rough surfaces, the roughness elements were glued with marine glue onto a 4.5 ± 0.1 mm thick acrylic plate. The characteristics of the roughness elements are presented in section 3.3.1.

As shown in Figure 3.2 (a), the Cartesian coordinate system was adopted in this study: the streamwise and wall normal directions are denoted by x and y respectively: $x = 0$ corresponds to the trailing edge of the step, $y = 0$ corresponds to the floor of the channel (for the smooth wall) or the crest of the roughness elements.

3.3.1 Roughness elements

With respect to the objective of this study, two rough surfaces were studied in addition to a reference smooth surface. The smooth surface facilitated the interpretation of the effects of surface roughness on the flow characteristics. Figure 3.3 shows the roughness elements used: (a) sand grains (hereafter referred to as *SG*) of average diameter 1.5 ± 0.2 mm and (b) wire mesh grit-80 (hereafter referred to as *WM*) with average wire diameter of 1.2 ± 0.15 mm and openness ratio of 27.2%. As indicated in section 3.3, the roughness elements were attached onto a 4.5 ± 0.1 mm thick acrylic plate using marine glue. Each of these roughness elements spanned the entire width of the channel and covers up to 1200 mm downstream of the trailing edge of the BFS. It should be noted that the upstream of the BFS was not covered with the roughness element for the rough surface cases so as to have the same approach flow conditions for the smooth and rough test cases. This facilitated the interpretation of roughness effects on the flow downstream of the BFS.

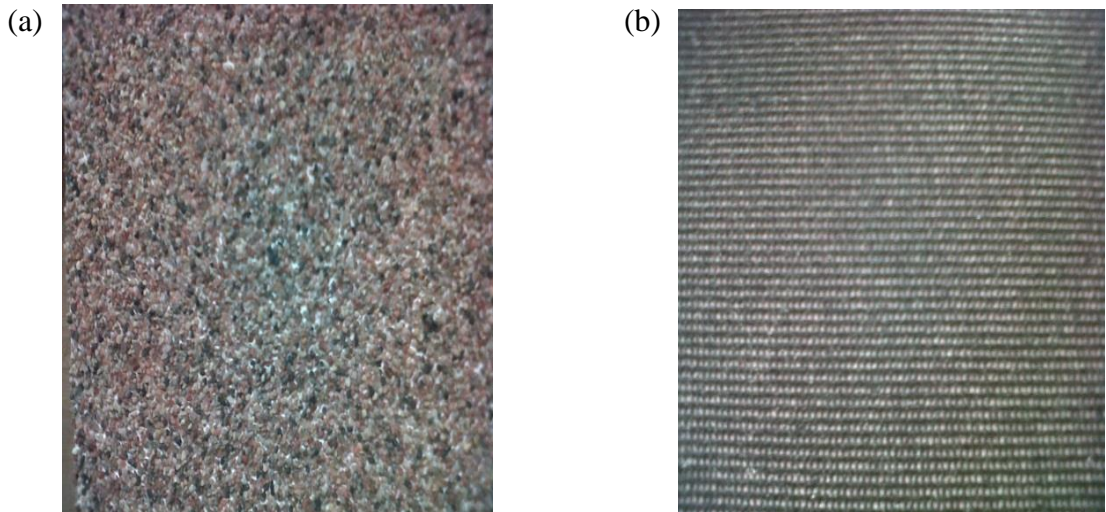


Figure 3.3: Roughness elements used to study surface roughness effects: (a) sand grain (b) wire mesh grit-80

3.4 Measurement procedure

Particle image velocimetry (PIV) technique was used to measure the velocity field of the flow. The PIV technique was employed because it is a non-intrusive multi-point velocity measurement technique. Unlike hotwire and pitot tube, the PIV is directional sensitive. This makes it possible to accurately determine both negative and positive velocities in the recirculation region of the flow in this study.

A schematic of a typical setup of a PIV system is shown in Figure 3.4. The setup consists of an optically transparent test section, flow seeded with seeding particles, laser to illuminate the seeding particles in the flow field, charged coupled device (CCD) camera to record the scattered light from the illuminated seeding particles, a synchronizer to control the camera and the laser, and computer with a suitable software to record, store and post process the recorded images. In the subsequent section the working principle of PIV technique is presented.

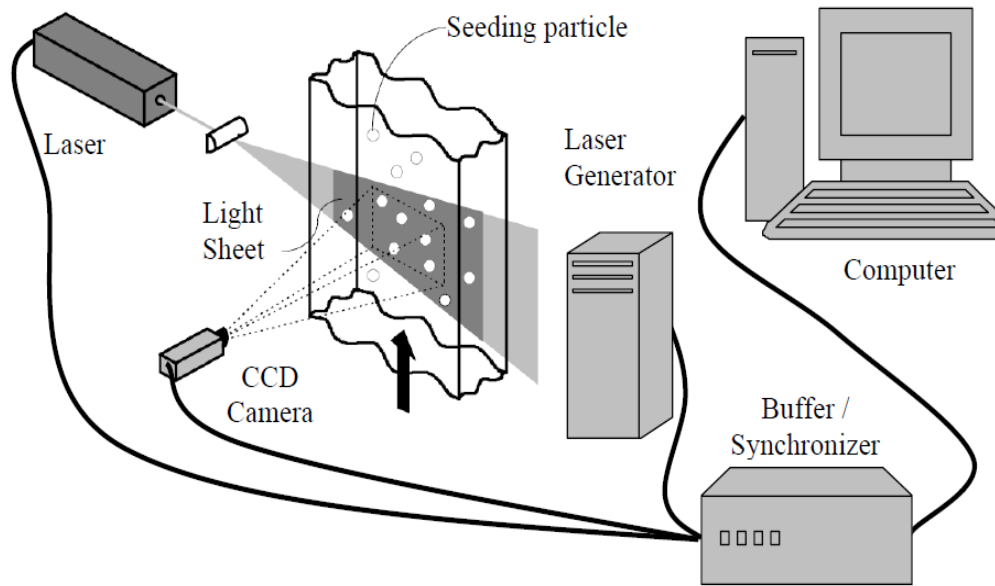


Figure 3.4: Schematic of a typical setup of a PIV system (Source: Shah, 2008)

3.4.1 Working principle of PIV

In PIV technique, the flow is seeded with tracer particles which are assumed to faithfully follow the flow dynamics. The flow with seeding particles is illuminated by two pulses of laser sheet separated by a time delay, Δt . The light scattered by the seeding particles is recorded and two successive images are captured. The images captured are then divided into grids of interrogation area (IA). For each IA, a numerical correlation algorithm is applied to statistically determine the local displacement vector (Δs) of the particles between the first and the second illuminations. The velocity, v_i , for a particular interrogation area is then obtained from the expression $v_i = \Delta s / \Delta t$. A velocity vector map over the whole target area is obtained by repeating the correlation for each interrogation area over the two image frames captured. In PIV technique, the flow field is analyzed at once to provide simultaneous whole-field measurement. The subsequent section gives description of the characteristics of the seeding particles, the light source and the recording medium used in a typical PIV system.

3.4.1.1 Seeding particles

The seeding particles should be small enough to follow the flow faithfully but large enough to scatter sufficient light for them to be detected by the camera. Also, the seeding particles should be distributed homogeneously (Westerweel *et al.*, 1996). Since PIV measures the velocity of the particle but not the fluid velocity, it is essential that the particles have certain hydrodynamic properties to ensure that they faithfully follow the flow. Particles that have negligible settling velocity are desirable. The settling velocity (v_s) can be estimated from Stokes law for flow around a sphere under gravity and is given by (Mei *et al.*, 1991):

$$v_s = \frac{(\rho_p - \rho_f)gd_p^2}{18\mu_f} \quad (3.1)$$

where ρ_p is the particle density, ρ_f is the fluid density, g is the acceleration due to gravity, d_p is the diameter of the particle and μ_f is the dynamic viscosity of the fluid.

The ability of a particle to follow the flow is characterized by its response time. The response time is a measure of the tendency of the particles to attain velocity in equilibrium with the fluid. The response time (τ_r) for the particle is given by (Raffel *et al.*, 1998):

$$\tau_r = \rho_p \frac{d_p^2}{18\mu_f} \quad (3.2)$$

The particles must also be good at scattering light to ensure that they are visible to the CCD sensor (Willert and Gharib, 1991). The particle size and shape, the refractive index and the wavelength of radiation are the factors that affect the light scatter by a particle. A variety of seeding particles are commercially available ranging from few microns to hundreds of microns. Some of the widely used particles for liquids are

polyamide seeding particles, silver-coated hollow glass spheres, hollow glass spheres, polystyrene latex and fluorescent polymer particles.

3.4.1.2 Light source

For PIV measurements, a high intensity laser is required to freeze the motion of the particles during image capturing. The fact that the whole field is illuminated and the camera captures the sideward scattered light by the particles makes a high power laser necessary. Frequency doubled neodymium-yttrium-aluminum-garnet (Nd:YAG) lasers are commonly used for PIV measurements because these lasers provide monochromatic light with high intensity illumination. Laser-emitted light is passed through a lens system to create a plane sheet of light to illuminate the region of interest. The length and width of the light sheet can be adjusted to the field of view required.

3.4.1.3 Recording medium

The CCD camera is the most widely employed recording device for PIV. CCD cameras have several advantages over photographic film cameras. These advantages include higher frame rates and possibility of on-line image analysis. However, photographic film cameras do offer higher resolution. The major component of a CCD camera is the CCD sensor which consists of an array of detectors called pixels. The CCD camera employed in the PIV studies generally uses high-performance progressive scan interline CCD chips. The chip consists of an array of photosensitive cells and an equal number of storage cells. After the first laser pulse is triggered, the first image is acquired and immediately transferred from the photosensitive cells to the storage cells. Later, when the second laser pulse is triggered, the photosensitive cells are available to store the second image. In this case, the storage cells contain the

first image and the photosensitive cells contain the second image. Then both images are transferred sequentially from the camera to the computer for storage. This allows the exposure interval Δt to be reduced to less than a microsecond. The subsequent section gives the PIV measurement procedure in the present study.

3.4.2 PIV measurement procedure in present study

In the present study, the flow was seeded with fluorescent polymer particles (Rhodamine - B) which is spherical in shape and of mean diameter $10\ \mu\text{m}$, specific gravity of 1.19 and refractive index of 1.479. The fluorescent polymer particles were chosen because its distribution is homogeneous. The settling velocity of the particles was estimated from equation 3.1 to be 1.04×10^{-5} m/s, which is far less than the velocity of the flow. Also, the particle response time was estimated from equation 3.2 to be 6.61×10^{-6} sec. The settling velocity and the response time show that the seeding particles indeed followed the flow dynamics faithfully.

The flow field with the seeding particles was illuminated with a 15 Hz repetition rate Nd-YAG double-pulsed laser with pulse energy of 120 mJ that emits green light at a wavelength of 532 nm. The laser sheet was shot above the channel with the light sheet aligned with the mid-span of the channel to obtain the x - y plane measurement.

A 12 bit 2048 x 2048 pixel charge coupled device (CCD) camera with a $7.4\ \mu\text{m}$ pixel pitch was used to capture the scattered light from the seeding particles. The camera was fitted with 60 mm Nikkor lens combined with an orange bandpass filter of wavelength 590 nm. The field of view used for all the planes of measurement is $83\ \text{mm} \times 83\ \text{mm}$. This field of view made it possible to capture the separated and reattachment regions of the flow. The images captured were post processed using adaptive correlation and moving average validation options of

DynamicStudio version 2.30 (commercial software developed by Dantec Dynamics Inc.). The adaptive correlation uses a multi-pass fast Fourier transform cross-correlation algorithm to determine the average particle displacement within an interrogation area. A three-point Gaussian curve fit was used to determine particle displacement with subpixel accuracy. The moving average validation validates or rejects vectors based on a comparison between neighboring vectors. The rejected vectors are then replaced by vectors estimated from surrounding values. It should be noted that in all the planes for the three test cases, the number of substituted velocity vectors in the main flow domain were less than 2%, which gives the indication that the PIV parameters were properly chosen. An interrogation area (IA) size of 32×32 pixels with 50% overlap was employed to process the instantaneous velocity data. The average number of particles in an interrogation area was 8. With the (IA) size of 32×32 pixels with 50% overlap, the maximum particle displacement in the mean flow direction was 8 pixels. The particle image diameter was estimated to be $1.13 \mu\text{m}$ (1.76 pixels), which is close to 2 pixels recommended by Raffel *et al.*, (1998) to minimize signal-to-noise ratio to ensure high quality data.

3.5 Test conditions

As shown in Figure 3.2(a), a trip made of wire mesh grit-80 was placed at the leading edge of the BFS with the aid of a double sided tape to enhance a rapid development of the approach turbulent boundary layer. The trip was 100 mm wide and spanned the entire width of the channel. The approach water depth (D) was maintained approximately at 70 mm for the three test cases. The approach free stream velocity of the flow was approximately 0.359 m/s for the three test cases. Based on the water depth and the free stream velocity, the Froude number (Fr) of the flow was estimated

as 0.43 and the Reynolds number of the flow was estimated as 25130. Thus the approach flow is in the turbulent and subcritical regime.

As shown in Figure 3.2(a), data were acquired for each test case at the upstream and downstream of the BFS: plane P0 is located at the upstream of the BFS and planes P1, P2, P3 and P4 are located in the downstream of the BFS. Results from Plane P0 were used to characterize the approach boundary layer prior to separation. Plane P1 results were used to characterize the separated and the reattachment regions of the flow whereas results from planes P2 to P4 were used to characterize the recovery region of the flow.

3.6 Convergence test

A convergence test was carried out to determine the sample size of image pairs required to accurately compute the mean and turbulent statistics in the present study. A sample size of $N = 1000, 3000$ and 5000 were used to calculate the mean velocity, Reynolds stresses and triple velocity correlations at various regions of the flow for the three test cases. Figure 3.5 shows the profiles obtained for the mean and turbulent quantities over the smooth surface. As shown in Figure 3.5, for each quantity, a comparison is made for the various sample sizes in the separated region at $x^* = x/x_r = 0.5$ (where x_r is the reattachment length) and the recovery region at $x^* = 7$. These locations correspond to $x/h \approx 2.6$ and $x/h \approx 36$ respectively. It was observed that the profiles for $N \geq 3000$ collapsed reasonably well. Hence, 5000 image pairs were used to compute the mean and turbulence statistics reported in this study. The number of image pairs used in the present study is substantially larger than those used to compute the mean and turbulent statistics in previous studies. For example, Piirto *et al.* (2003) used 510 image pairs to compute the mean velocity, Reynolds

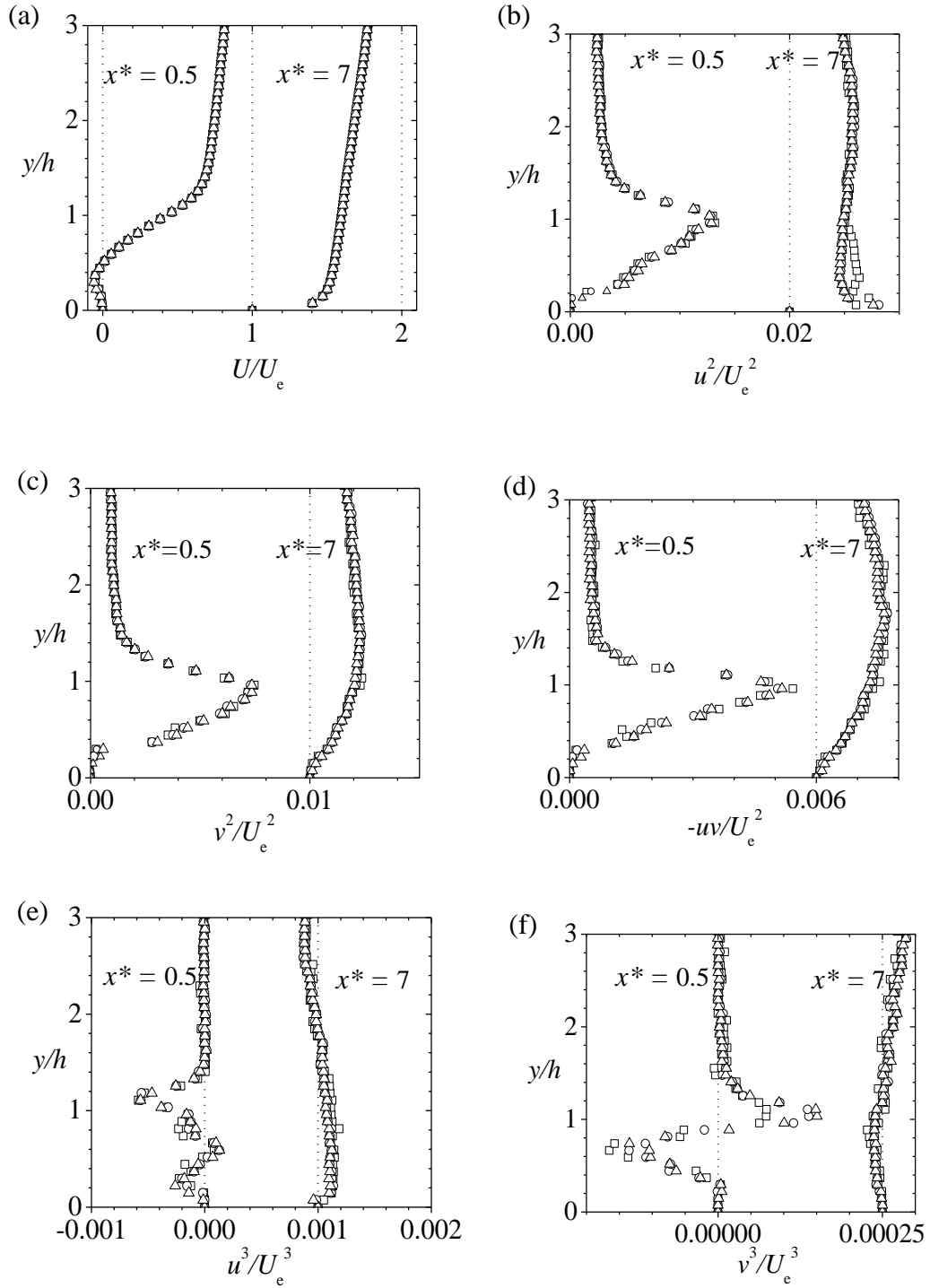


Figure 3.5: Profiles of mean and turbulent quantities obtained in the separated region ($x^* = 0.5$) and the recovery region ($x^* = 7$) using $N = 1000$ (\square), 3000 (\circ), 5000 (Δ): (a) U/U_e (b) u^2/U_e^2 (c) v^2/U_e^2 (d) $-uv/U_e^2$ (e) u^3/U_e^3 (f) v^3/U_e^3

stresses and the various transport terms in turbulent kinetic energy equation in separated and reattached flow downstream of a backward facing step. Also, Shah (2008) used 2040 image pairs to compute the mean velocity, turbulence intensities, Reynolds shear stress, triple velocity correlation and the various transport terms in turbulent kinetic energy equation in separated and reattached flow downstream of a rib.

3.7 Measurement uncertainty

The measurement uncertainty in the data of this study was estimated following the AIAA standard derived and explained by Coleman and Steele (1995). In general, the total error is composed of two components: a precision component and a bias component. Coleman and Steele (1995) classified an error as precision if it contributes to the scatter of the data and systematic error is a bias error. On basis of the size of interrogation area and Gaussian curve fit used to calculate the instantaneous vector maps, and the large number of instantaneous vector maps used to calculate the mean velocity and turbulent quantities, at 95% confidence level, the uncertainties in the mean velocities, turbulence intensities, Reynolds stresses, triple velocity correlations and production term of turbulent kinetic energy equation were estimated to be $\pm 2\%$, $\pm 5\%$, $\pm 10\%$, $\pm 15\%$ and $\pm 15\%$, respectively.

CHAPTER 4

RESULTS AND DISCUSSION

The characteristics of the mean flow and the turbulence field of the three sets of experiments are presented and discussed in this chapter. The discussion is structured into three main sections. The first section focuses on the characteristics of the approach flow in the upstream region before separation. The second section discusses surface roughness effects on the flow characteristics in the separated and reattachment regions, and the third section examines the effects of surface roughness on the characteristics of the flow in the recovery region.

4.1 Flow characteristics in the upstream region

As indicated in section 2.4.1, the characteristics of the approach flow have a significant impact on the dynamics of the flow downstream of the BFS. Also, in numerical studies of turbulent flow over BFS, the approach flow characteristics will be vital for setting inlet boundary conditions. In the present study, the approach flow was characterized by the distributions of the streamwise mean velocity and the turbulence intensities, as well as the shape factor, skin friction coefficient and the Coles wake parameter. The profiles for the mean velocity and the turbulence intensities are presented in both inner and outer coordinates. It should be recalled that the friction velocity (U_τ) and viscous length (ν/U_τ) are respectively the velocity scale and length scale for inner coordinates, whereas the freestream velocity (U_e) and the boundary layer thickness (δ) are respectively the velocity scale and length scale for the outer coordinates. Figure 4.1(a) shows the distribution of the streamwise mean velocity in outer coordinates. As expected, the streamwise mean velocity varies from the no-slip condition at the wall ($y = 0$) to its freestream value at the edge of the

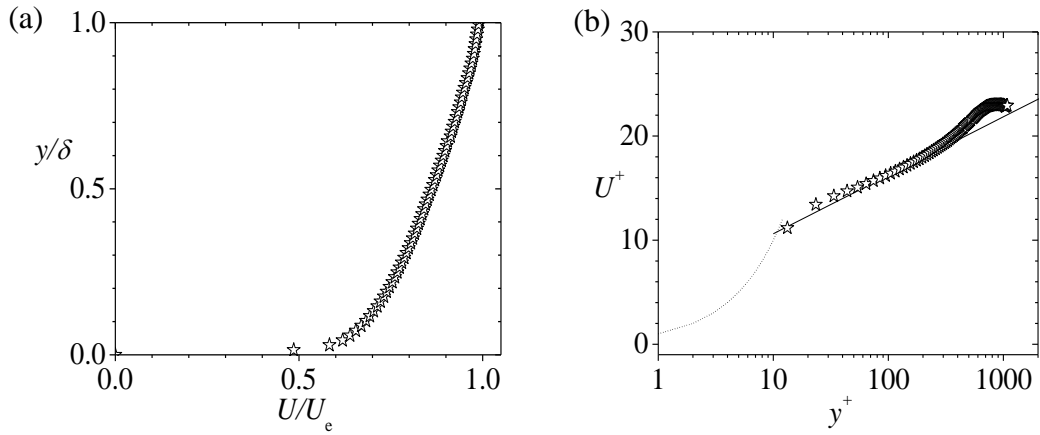


Figure 4.1: Mean velocity profiles in (a) outer coordinates, (b) inner coordinates. The law of the wall (dotted line) and logarithmic law with $\kappa = 0.41$ and $B = 5.0$ (solid line) are shown for comparison

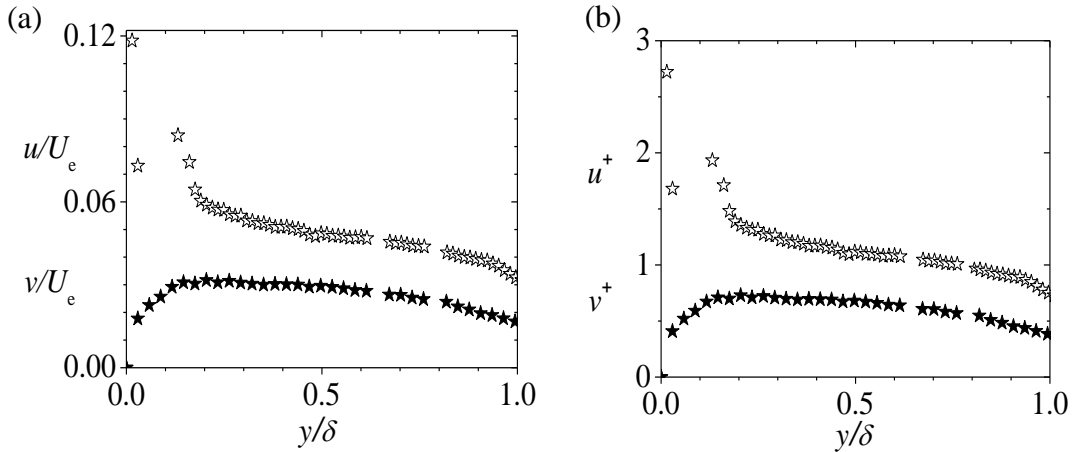


Figure 4.2: Turbulence intensities and Reynolds shear stress in (a) inner coordinates (b) outer coordinates

boundary layer ($y = \delta$). The variation of the mean velocity with wall normal distance is most dramatic in the immediate vicinity of the wall, where viscous effects are most dominant. As remarked earlier in section 2.2, the ratio of the mass displacement to momentum thickness associated with the boundary layer defines the shape factor (H) of the mean velocity profile. The magnitude of the displacement thickness and the momentum thickness determined in the present study are 6.68 mm and 4.67 mm respectively. Hence, the shape factor of the profile was determined to be 1.43. The

value of H compares favorably with 1.4 observed at similar Reynolds number ($Re_\theta = 1680$) for ZPG turbulent boundary layer (Purtell *et al.*, 1981; Monkewitz *et al.*, 2008).

Figure 4.1(b) shows the streamwise mean velocity profile in inner coordinates. That is, the streamwise mean velocity was fitted onto the classical logarithmic law ($U^+ = \kappa^{-1} \ln y^+ + B$). The logarithmic law constants adopted in this plot are $\kappa = 0.41$ and $B = 5.0$. The mean velocity data is well described by the logarithmic law in the region $30 \leq y^+ \leq 370$. By fitting the streamwise mean velocity data onto the logarithmic law, the friction velocity was determined for the estimation of the skin friction coefficient. The value of the skin friction coefficient was determined from the relation $C_f = 2(U_\tau/U_e)^2$ to be 0.0038. The value of C_f in the present study compares well with 0.004 observed in prior open channel turbulent flow (Afzal *et al.*, 2009) but is about 7% higher than the value obtained at similar Reynolds numbers in ZPG turbulent boundary layer (Purtell *et al.*, 1981; Fernholz and Finley, 1996). The higher value of C_f in the present study and prior open channel turbulent flows than that observed in the ZPG turbulent boundary layer at similar Reynolds number may be attributed to the characteristic high background turbulence in open channel turbulent flows. In the present study the turbulence level (u/U_e) at the edge of the boundary layer was 4%, which is higher than typical values of 0.5% in ZPG turbulent boundary layer.

From Figure 4.1(b), the outer region of the boundary layer was examined by determining the strength of the Coles wake parameter, II . The strength of the Coles wake parameter is related to the maximum deviation of the measured mean velocity (ΔU^+) in the outer region from the logarithmic law as $\Delta U^+ = 2II/\kappa$

(Fernholz and Finley, 1996). In the present study, a wake parameter of magnitude 0.2 was determined. This value agrees with prior open channel turbulent flow studies (Tachie *et al.*, 2003; Afzal *et al.*, 2009) but is lower than values obtained at similar Reynolds numbers in ZPG turbulent boundary layers. For instance, at a similar Reynolds number in ZPG turbulent boundary layer, Purtell *et al.* (1981) obtained a Π value of 0.41. The relatively lower value in the present study and previous open channel turbulent flows than that observed for ZPG turbulent boundary layer is also attributed to the characteristic higher turbulence level in open channel turbulent flows.

The turbulence field of the approach flow was analyzed using the streamwise turbulence intensity (u) and wall normal turbulence intensity (v). The profiles of the streamwise turbulence intensity (u) and wall normal turbulence intensity (v) normalized with U_e and U_τ are presented respectively in Figure 4.2(a) and Figure 4.2(b). In both figures the boundary layer thickness was used as the length scale. The respective peak values $u^+ = 2.75$ and $u/U_e = 0.12$ are consistent with values obtained in prior open channel study (Tachie *et al.*, 2003), ZPG turbulent boundary layer (Ching *et al.*, 1995) and approach flow of separated and reattached turbulent flows with ZPG (Kasagi and Matsunaga, 1995; Piirto *et al.*, 2003) and open channel (Nakagawa and Nezu, 1987; Agelinchaab and Tachie, 2008). The peak values of u^+ and u/U_e occur in the inner layer at $y/\delta = 0.01$ which is consistent with observation made by Tachie *et al.* (2003) in open channel turbulent flow study and Ching *et al.* (1995) in ZPG turbulent boundary layer study. From Figure 4.2, the respective peak values of $v^+ = 0.8$ and $v/U_e = 0.03$ are observed for the wall normal turbulence intensity which are less than 1.1 and 0.04 respectively observed for high Reynolds number asymptote in canonical near wall turbulent flows (Fernholz and Finley, 1996; Monkewitz *et al.*, 2008). This is not surprising because in

prior studies of turbulent boundary layers, the wall normal turbulence intensity was observed to be influenced by factors such as low Reynolds number and freestream turbulence, thereby causing variation in the peak values (Fernholz and Finley, 1996).

4.2 Roughness effects in the separated and the reattachment regions

In this section, roughness effects on mean flow parameters (which include the reattachment length, maximum negative streamwise mean velocity, growth rate of vorticity thickness and the profiles for the streamwise and wall normal mean velocities), the profiles for the Reynolds stresses, Reynolds stress ratios, turbulence kinetic energy, turbulence energy production and triple velocity correlation in the separated and the reattachment regions are presented.

4.2.1 Mean flow characteristics

4.2.1.1 Contour of streamwise mean velocity and mean streamlines

Contour plots of the streamwise mean velocity in the separated and reattachment regions with the mean streamlines superimposed on them were obtained for the three test cases to study the salient features of the mean flow in these regions. The results obtained for the three test cases were qualitatively similar, hence only the plots for the smooth surface (Figure 4.3(a)) and wire mesh roughness (Figure 4.3 (b)) are presented. The freestream velocity of the approach flow (U_o) was used as the velocity scale to normalize the streamwise mean velocity, and the step height h was adopted as the length scale for normalizing both the wall normal distance and the streamwise distance. As expected, the flow separated at the trailing edge of the step and reattached at some distance downstream of the step. There was also a formation of a distinct recirculation region. In the recirculation region, the streamline plots reveal a primary recirculation and a corner eddy, which is consistent with prior studies of

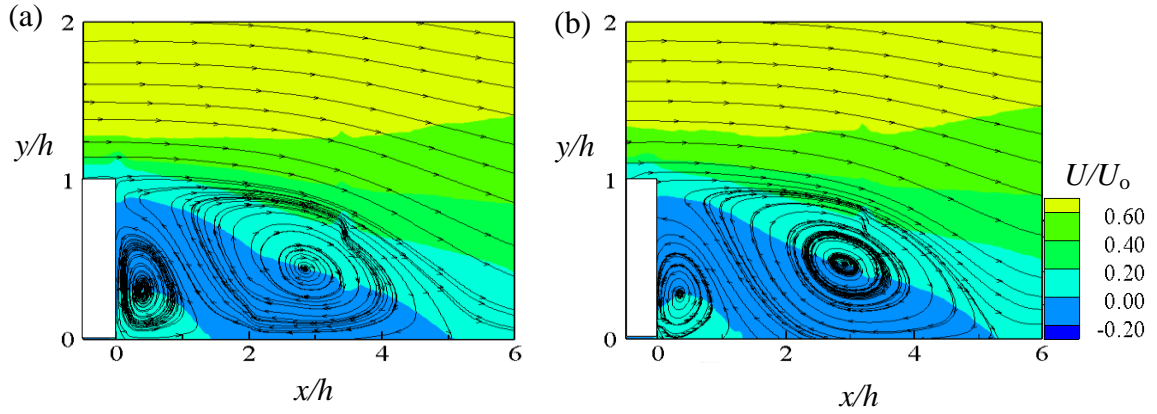


Figure 4.3: Distribution of mean streamwise velocity with mean streamlines in the separated and the reattachment regions for (a) *SM* and (b) *WM*

separated and reattached turbulent flows over smooth surface with ZPG (Kostas *et al.*, 2002) and open channel (Agelinchaab and Tachie, 2008). Consistent with prior studies of separated and reattached turbulent flows, the lower half of the recirculation region is dominated by reverse flow. Significant values of negative velocity over the smooth and rough surfaces were obtained in the recirculation region. The magnitude of the maximum negative velocity is about $0.12U_o$ over both the smooth and rough surfaces. This value is less than $0.2U_o$ usually reported for flows over BFS with ZPG (Kassagi and Matsunaga, 1995) but it is in good agreement with $0.1U_o$ observed for flows over BFS in open channel (Nakagawa and Nezu, 1987).

The reattachment location for the separated shear layer was estimated from the mean streamlines as the streamwise location at which the mean dividing streamline from the trailing edge of the BFS ($y = 1, x = 0$) reattached onto the wall. The reattachment length observed for the smooth (*SM*), wire mesh (*WM*), and sand grain (*SG*) was $5.2h$, $5.2h$ and $5.3h$, respectively. An independent estimate of the reattachment length was also made by using the forward fraction method. That is determining the streamwise location where the forward fraction of the streamwise mean velocity at the wall is 0.5. The forward fraction method produced reattachment length of

5.1*h*, 5.2*h* and 5.2*h* respectively for *SM*, *WM* and *SG*. The difference in the reattachment lengths obtained from both methods for a given surface condition is within a measurement uncertainty of $\pm 0.3h$. Also, the reattachment length does not show any significant surface roughness effect. The magnitude of the reattachment length observed for the three test cases from the two methods is about 20% less than a reattachment length of 6.5*h* observed for turbulent flow over BFS with ZPG (Adams and Johnston, 1988; Kasagi and Matsunaga, 1995) but compares well with reattachment length of 5*h* observed for turbulent flows over BFS in an open channel (Nakagawa and Nezu, 1987). It should be noted that the approach flow of the present study and that of the prior studies mentioned were fully turbulent. As demonstrated by Adams and Johnston (1988) and Piirto *et al.*, (2003), when the approach flow is fully turbulent, Reynolds number and perturbation strength have no significant effects on the reattachment length. Therefore, the reduction in the reattachment length in the present study and that of Nakagawa and Nezu (1987) compared to that observed by Adams and Johnston (1988) and Kasagi and Matsunaga (1995) may be attributed to the relatively high background turbulence associated with open channel.

4.2.1.2 Growth of separated shear layer

As mentioned earlier in section 1.2.2 of chapter one, when the approach boundary layer separates from the wall, there is a formation of a thin shear layer in the separated region. The separated shear layer was analyzed using the growth rate of vorticity thickness. This method was applied by Jovic (1996) in separated and reattached turbulent flows over BFS with ZPG and Agelinchaab and Tachie (2008) in separated and reattached turbulent flows over square, semicircular and rectangular prisms in open channel. The vorticity thickness is given by $\delta_\omega = \Delta U / (dU/dy)_{\max}$, (where ΔU is the maximum velocity difference). The distribution of ΔU and $(dU/dy)_{\max}$ is presented

in Figure 4.4(a) and Figure 4.4(b) respectively. In Figure 4.4(a-b), the freestream velocity (U_o) of the approach flow was used as the velocity scale, the step height was used as the length scale for normalizing the wall normal distance and the reattachment length (x_r) was used as the length scale for normalizing the streamwise distance. Figure 4.4(a) shows that the velocity difference increases to 1.12 at about $x^* = 0.6$ and decreases to a value of unity at reattachment. The peak value of 1.12 compares favorably with 1.1 reported by Jovic (1996) in a study of turbulent flow downstream of a BFS at Re_h of 37000. Agelinchaab and Tachie (2008) observed 1.26 in a study of turbulent flows over rectangular, square and semicircular prisms in an open channel at Re_h of 1920 which is about 13% higher than that in the present study. As expected, the distribution of $(dU/dy)_{max}$ shows a systematic decrease as the flow evolves in the streamwise direction after separation.

The values of δ_w were evaluated for the three test surfaces and the distributions are presented in Figure 4.4(c). Surface roughness does not show any significant effect on the vorticity thickness of the shear layer. The vorticity thickness increases almost linearly with streamwise distance, which agrees qualitatively with that of a plane mixing layer. However, the slope, which represents the growth rate of vorticity thickness was determined to be approximately 0.23, which is higher than the values in the range of 0.15 to 0.22 observed for a plane mixing layer (Brown and Roshko, 1974). The present growth rate for the vorticity thickness is about 27% lower than the value reported by Agelinchaab and Tachie (2008) in a study of turbulent flows over rectangular, square and semicircular prisms in an open channel at Re_h of 1920. The approach flow characteristics are similar in the present study and that of Agelinchaab and Tachie (2008). Therefore, it may be deduced that

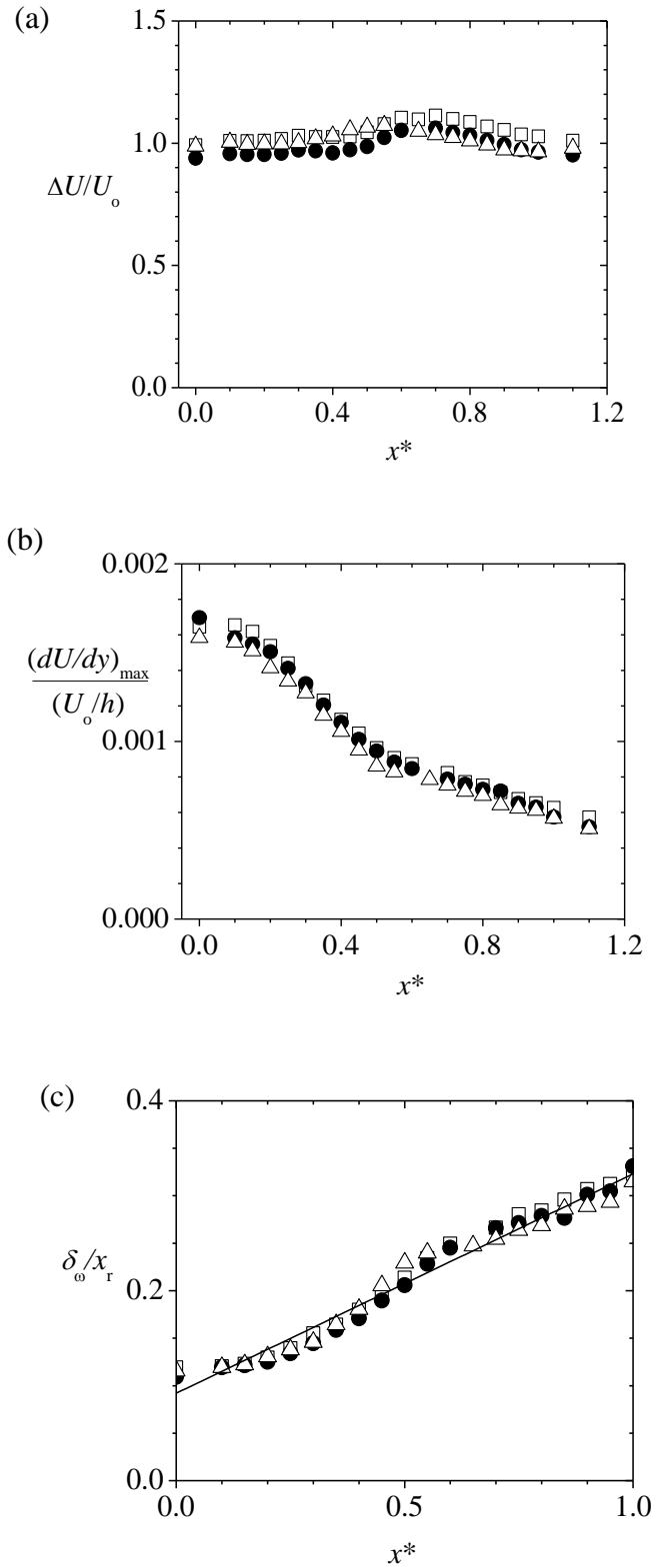


Figure 4.4: Distribution of (a) maximum velocity difference, (b) maximum slope, (c) growth rate of vorticity thickness in the separated and the reattachment regions. Symbols: \square SM \triangle WM \bullet SG

the growth rate of vorticity thickness in the separated shear layer is geometry dependent.

4.2.1.3 Mean velocity profiles

Surface roughness effects on the distributions of the profiles for the streamwise mean velocity and wall normal mean velocity were examined in the separated and the reattachment regions at the following selected streamwise locations: $x^* = 0.25, 0.5, 0.75$ and 1. The same locations are used in subsequent plots shown for the separated and reattachment regions. The mean velocities were normalized with the local freestream velocity, U_e , which is shown in Figure 4.5 and the wall normal distance was normalized with the step height (h). The profiles for normalized U and V are presented in Figure 4.6(a) and Figure 4.6(b) respectively. As expected, Figure 4.6(a) shows that profiles of U in the separated and reattachment regions are significantly distorted in the near wall region. However, as the flow evolves along the streamwise direction, the profiles become more uniform. The figure demonstrates that surface roughness has no significant effects on streamwise mean velocity profiles within the separated and the reattachment regions.

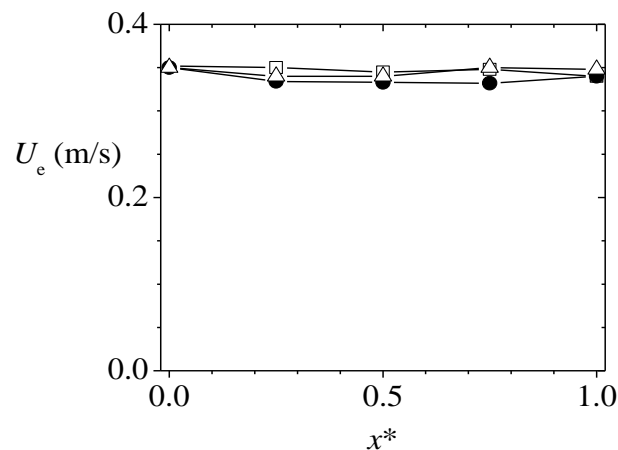


Figure 4.5: Distribution of local freestream velocity in the separated and reattachment regions Symbols: \square SM \triangle WM \bullet SG

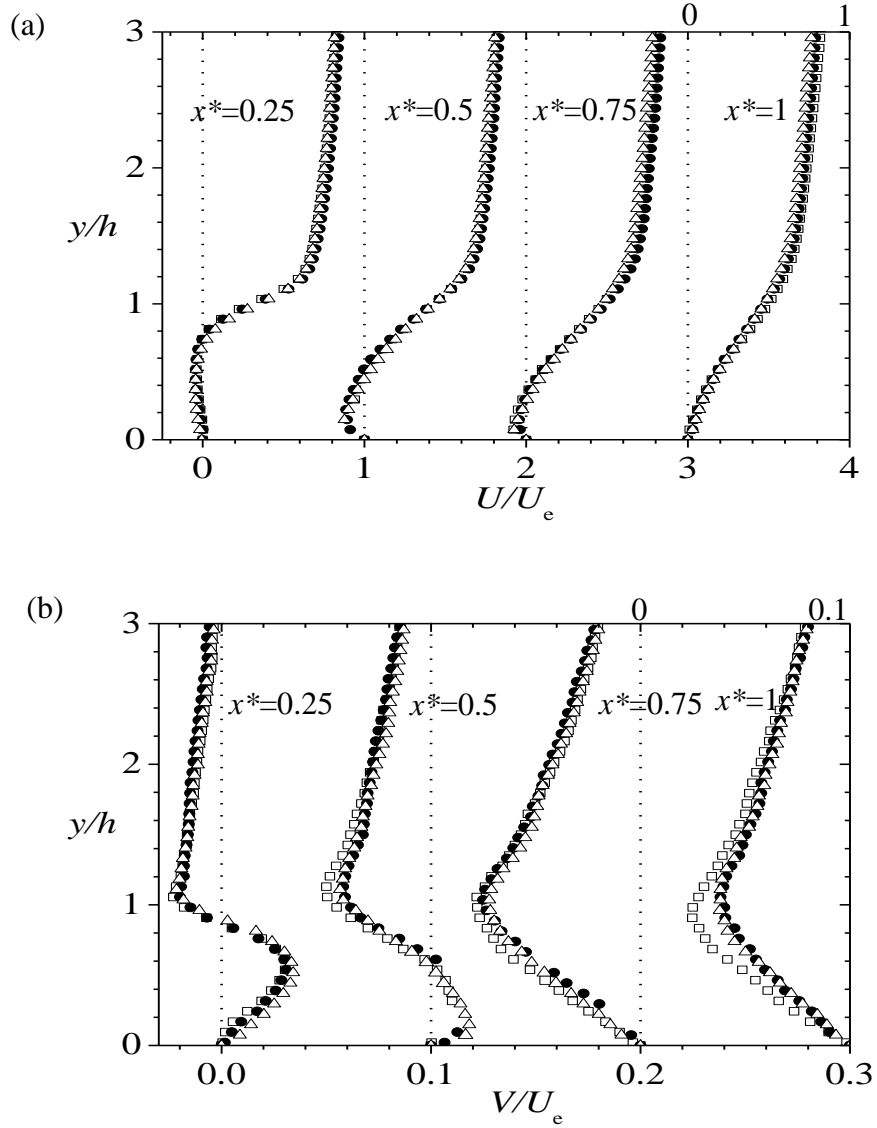


Figure 4.6: Mean velocity profiles (a) streamwise (b) wall normal in the separated and reattachment regions. Symbols: \square SM \triangle WM \bullet SG

In Figure 4.6(b), it is noted that the profiles for wall normal mean velocity for all the three test cases collapse reasonably well at the various streamwise location except for the reattachment location ($x^* = 1$), where the smooth and the rough surfaces do not collapse in the region $0.16 \leq y/h \leq 2$. At $x^* = 1$, the magnitude of SM profile at $y/h = 1$ is about 17% higher than that observed over SG and WM. The profiles of V in the separated and the reattachment regions exhibit significant negative magnitudes. For example at $x^* = 0.5$, the value of V is about $0.08U_e$ which compares reasonably well

with the maximum negative value observed for U . The magnitude of V observed in the separated and reattachment regions is consistent with observations made in prior studies of separated and reattached turbulent flows. For instance, Kasagi and Matsunaga (1995) observed a maximum value of V to be $0.08U_e$ for separated and reattached turbulent flow over a BFS with ZPG, Agelinchaab and Tachie (2008) observed a maximum value of V to be $0.08U_e$ for separated and reattached turbulent flow over a square rib in open channel and $0.25U_e$ was observed by Shah (2008) in separated and reattached turbulent flow over ribs with ZPG.

4.2.2 Reynolds stresses

The Reynolds stresses are associated with the mean rate of deformation which is vital to the sustenance of turbulence. The distribution of the Reynolds stresses at the selected streamwise locations is presented in Figure 4.7. Figure 4.7(a) shows the profiles for the streamwise Reynolds normal stress (u^2/U_e^2), Figure 4.7(b) shows the profiles for the wall normal Reynolds normal stress (v^2/U_e^2) and Figure 4.7(c) shows the profiles for Reynolds shear stress ($-uv/U_e^2$). The distribution of the Reynolds stresses is qualitatively similar but the magnitude of v^2/U_e^2 and $-uv/U_e^2$ is less than u^2/U_e^2 . The Reynolds stress distributions do not show significant surface roughness effect in the separated and reattachment regions. The profiles increase from zero, attain a peak and then decline as the freestream is approached. The peak values for u^2/U_e^2 and v^2/U_e^2 increase along the streamwise distance and attain maximum at the reattachment point whereas the Reynolds shear stress attains maximum peak values at about $x^* = 0.5$. The peak values of the Reynolds stresses observed for the three test cases are far higher than reported in canonical near wall turbulent flows and open channel turbulent flows. For example, at the reattachment point, the peak values

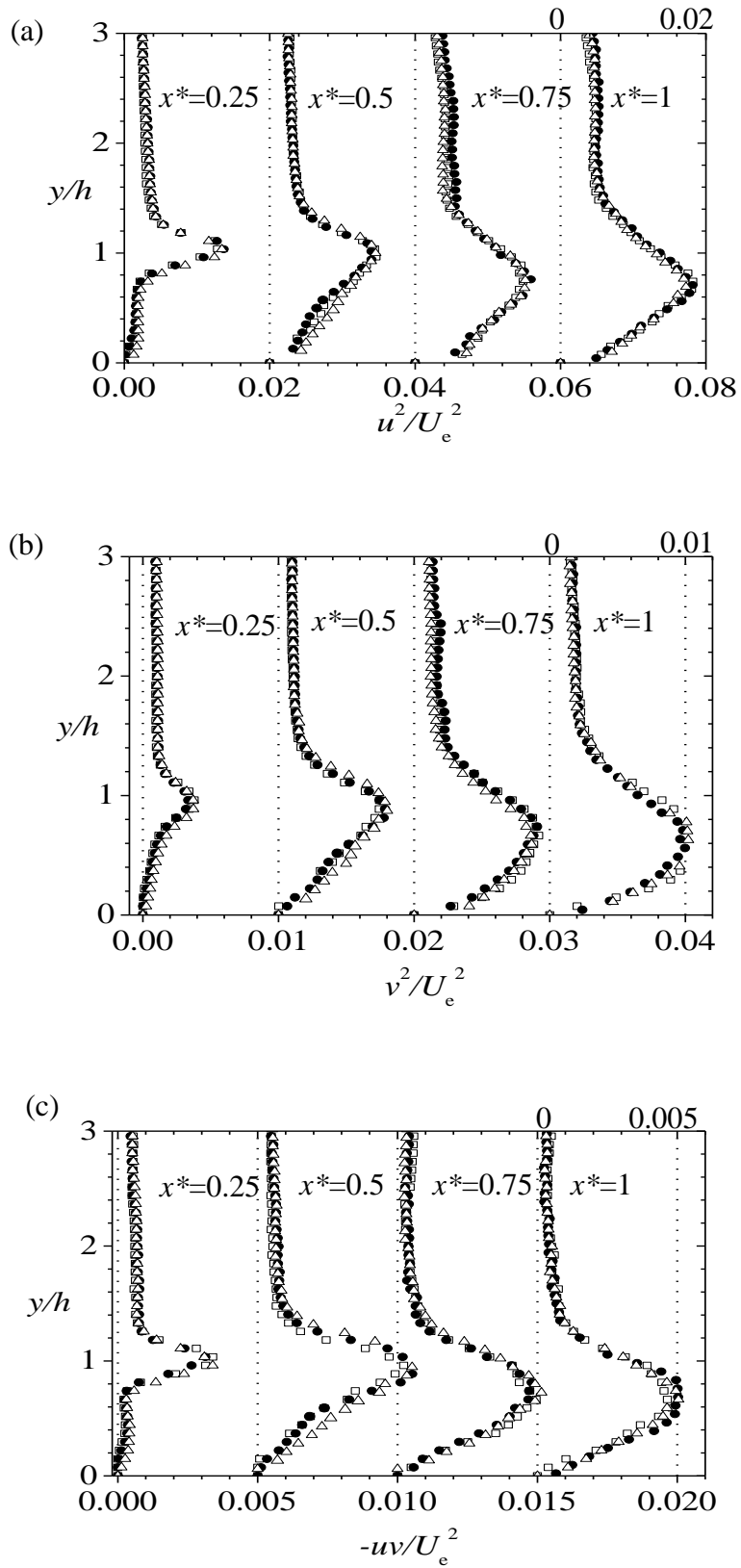


Figure 4.7: Reynolds stresses in the separated and reattachment regions: (a) u^2/U_e^2 (b) v^2/U_e^2 (c) $-uv/U_e^2$. Symbols: \square SM \triangle WM \bullet SG

observed for u^2/U_e^2 , v^2/U_e^2 and $-uv/U_e^2$ are about 28%, 84% and 80% respectively higher than that observed for canonical near wall turbulent flows (Fernholz and Finley, 1996) and open channel turbulent flows (Nezu and Rodi, 1986). This gives the indication that separated and reattached turbulent flows enhance turbulence more than canonical near wall turbulent flows and open channel turbulent flows. In comparison with previous studies of separated and reattached turbulent flows, it was observed that the Reynolds stress maxima in the separated and the reattachment regions vary. For example, the largest value of u^2/U_e^2 in the present study is about 0.018, which agrees reasonably with 0.02 observed by Kostas *et al.* (2002) in turbulent flows over BFS with ZPG at Re_h of 4660 but it is about 50% less than that observed by Kasagi and Matsunaga (1995) in turbulent flows over BFS at $Re_h = 5540$ with ZPG and that observed by Nakagawa and Nezu (1987) in turbulent flows over BFS in open channel at $Re_h = 8200$. For v^2/U_e^2 , the largest value of 0.01 in the present study is about 23% less than that observed by Kostas *et al.*, (2002) and 66% less than that observed by Nakagawa and Nezu (1987). Also for $-uv/U_e^2$, largest value of 0.005 was observed in the present study and it is about 50% less than that observed by Nakagawa and Nezu (1987) and Kostas *et al.* (2002). The Reynolds stress maxima in the present study were compared with that of Agelinchaab and Tachie (2008) in turbulent flows over square, semicircular and triangular prisms in open channel at Re_h of 1920. It was observed that the maximum value of u^2/U_e^2 in the present study is 38% higher than that observed for the semicircular and triangular prisms but 50% less than that observed for the square prism. For v^2/U_e^2 , the largest value in the present study compared reasonably with that observed for the semicircular and triangular prisms but 68% less than that observed for the square prism. The disparity in the magnitude of the

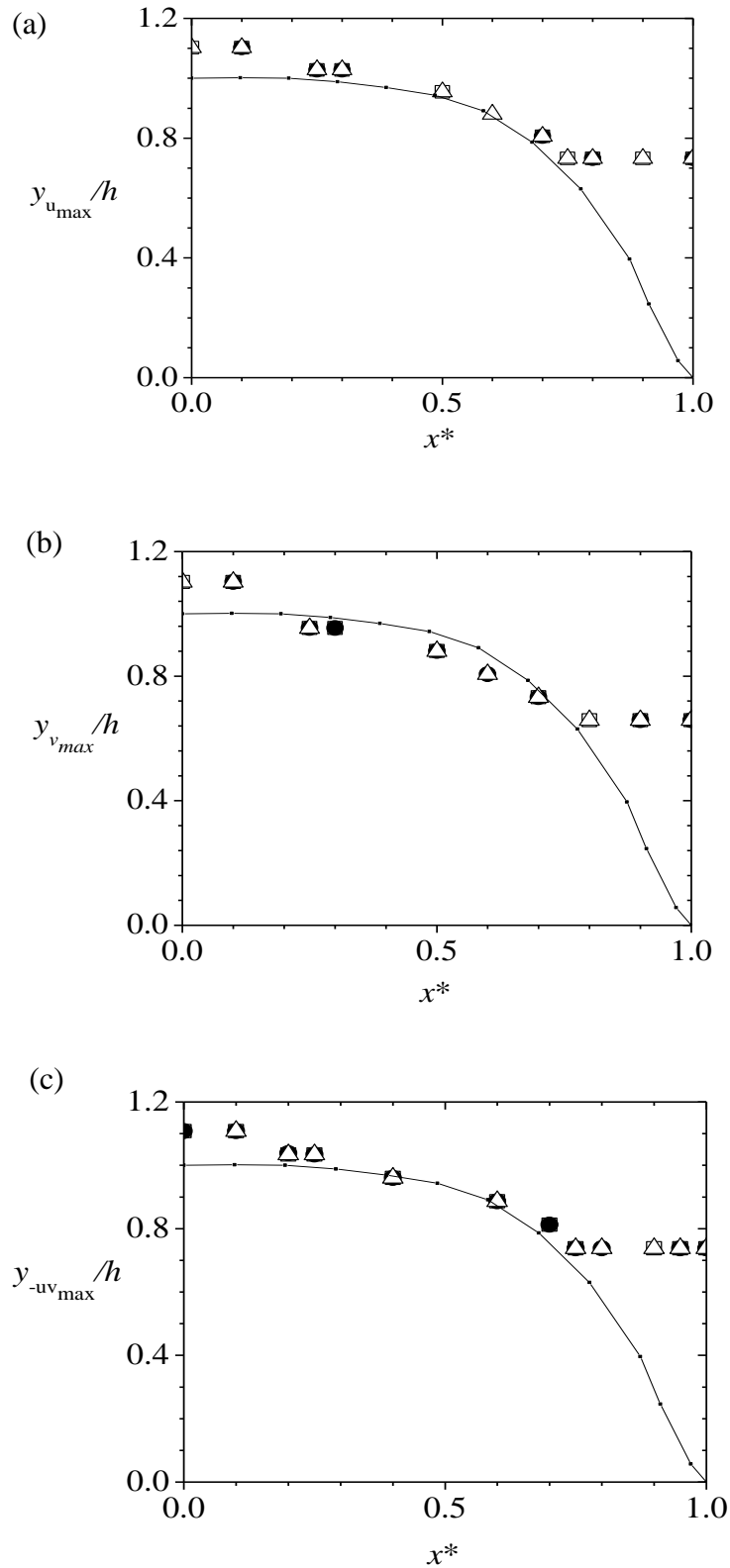


Figure 4.8: y -locations where peak values of (a) u^2/U_e^2 , (b) v^2/U_e^2 and (c) $-uv/U_e^2$ occur along the dividing streamline. Symbols: \square SM \triangle WM \bullet SG

Reynolds stress maxima in the present study and that of previous studies may be attributed to the variations in the boundary conditions and geometry for inducing flow separation.

Figure 4.8(a-c)) show the y/h locations where the peak values of u^2/U_e^2 , v^2/U_e^2 and $-uv/U_e^2$ for the three test cases occur. The dividing streamline for *SM* is also shown in these figures to visualize how the locations deviate from the dividing streamline. The location for the peak values of u^2/U_e^2 , v^2/U_e^2 and $-uv/U_e^2$ for the three test cases occur approximately along the dividing streamline in the range $0 \leq x^* \leq 0.8$ and moves away from the dividing streamline as the reattachment point is approached. The upper limit of $x^* = 0.8$ is in agreement with values reported for turbulent flows over BFS with ZPG at Re_h of 4660 (Kostas *et al.*, 2002) but higher than 0.5 observed for separated and reattached turbulent flow over ribs with ZPG at $Re_h = 2640$ (Shah, 2008). The variation in the geometry used to induce flow separation may explain the disparity in the upper limit observed in the present study and that of Shah (2008). Towards the reattachment point, the peak location moves close to the wall due to damping effects from the wall on the flow. However, the locations are farther away in comparison with canonical near wall turbulent flows and open channel turbulent flows.

4.2.3 Turbulence kinetic energy

The profiles of the turbulence kinetic energy (k) in the separated and reattachment regions are presented in this section. Turbulence kinetic energy is calculated from $k = 0.5(u^2 + v^2 + w^2)$. Since the spanwise Reynolds normal stress (w^2) was not measured in the present study, it was approximated as $0.5(u^2 + v^2)$. Substituting $w^2 = 0.5(u^2 + v^2)$ into $k = 0.5(u^2 + v^2 + w^2)$ yielded $k = 0.75(u^2 + v^2)$. Hence, the

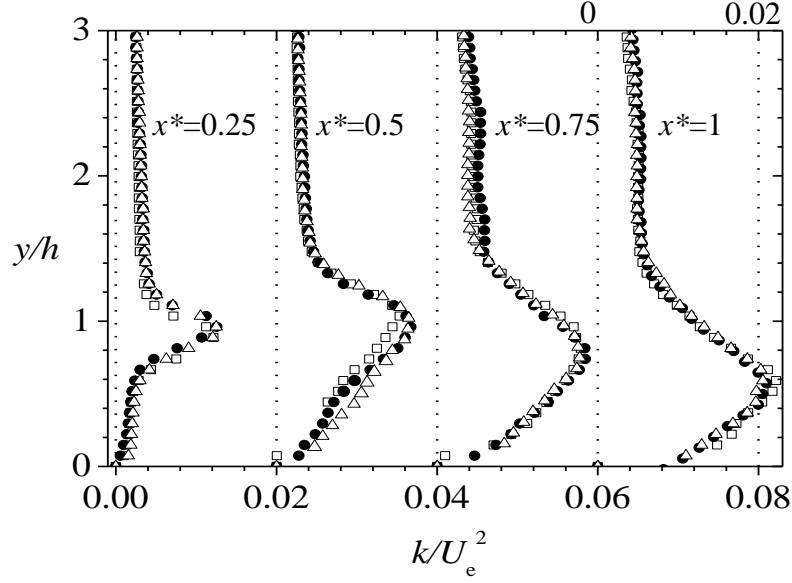


Figure 4.9: Turbulent kinetic energy in the separated and reattachment regions. Symbols: \square SM \triangle WM \bullet SG

profiles for turbulence kinetic energy in the present study was determined from $k = 0.75(u^2 + v^2)$ and are shown in Figure 4.9. Surface roughness effect is not significant on the turbulence kinetic energy distribution in the separated and reattachment regions. However, the level of the turbulence kinetic energy increases as the flow evolves from the point of separation and attains its peak at the point of reattachment. The highest value for the turbulence kinetic energy in the present study is about 38% less than that observed by Kasagi and Matsunaga (1995) in turbulent flows over BFS with ZPG. The disparity is not surprising since the Reynolds stress maxima in the present study and that of Kasagi and Matsunaga (1995) varied significantly (refer to section 4.2.2).

4.2.4 Reynolds stress ratios

In this section, the distributions of the ratio of the Reynolds normal stresses (v^2/u^2) and Townsend structure parameter (the ratio of the Reynolds shear stress ($-uv$) to twice the turbulence kinetic energy, $-uv/2k$) are presented. In standard two-equation

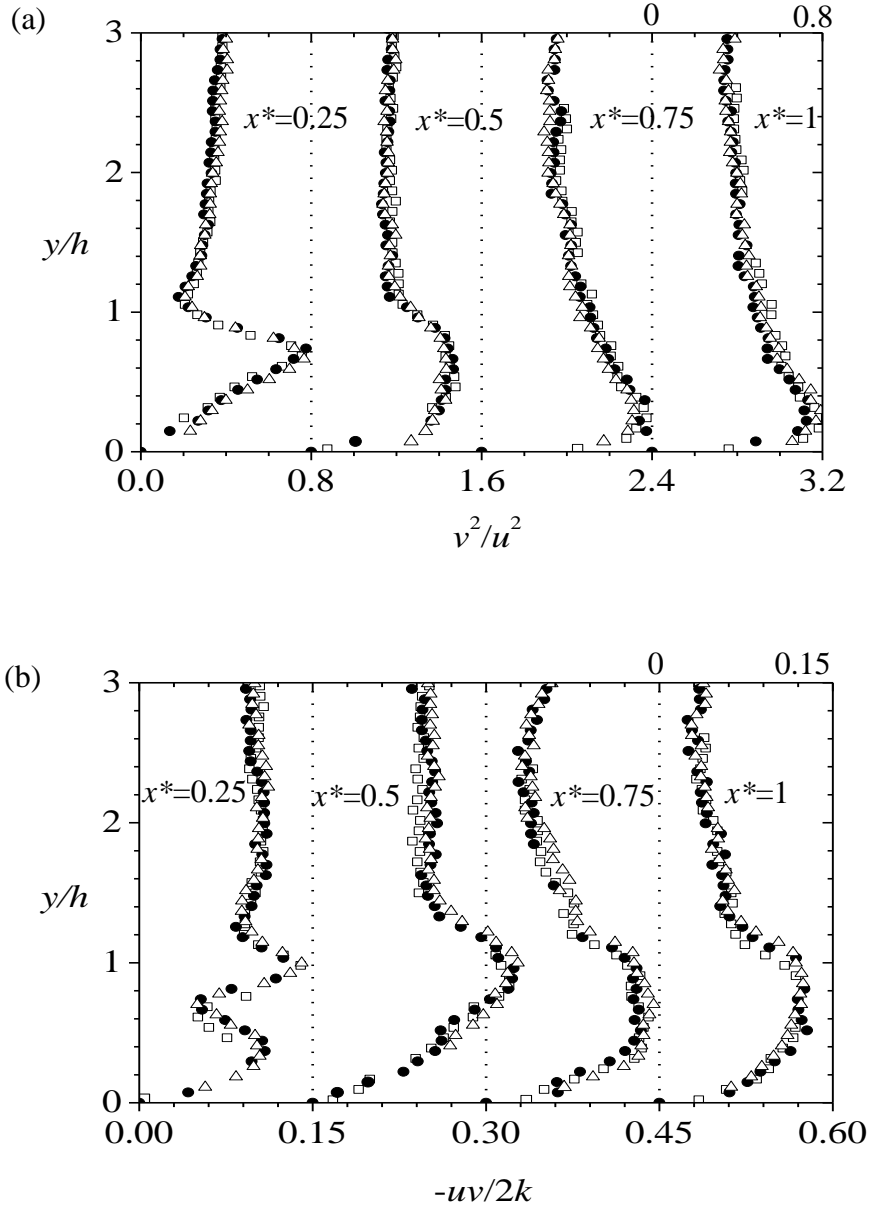


Figure 4.10: Distribution of (a) v^2/u^2 and (b) $-uv/2k$ at selected streamwise locations in the separated and reattachment regions. Symbols: \square SM \triangle WM \bullet SG

models (for example, k - ε and k - ω models) local isotropy (that is $v^2/u^2 = 1$) is assumed. The distribution of v^2/u^2 was examined in the present study to provide information on the large scale anisotropy of the flow. Profiles for v^2/u^2 at the selected streamwise locations in the separated and the reattachment regions are presented in Figure 4.10(a). At the various streamwise locations in the separated and the reattachment regions, surface roughness has no significant effect on the distribution of the large scale anisotropy of the flow. The distribution of v^2/u^2 increases from zero at

the wall and attains a peak value and then declines towards the freestream. The peak values at the various locations is about 0.8 except for the profile at $x^* = 0.5$ which is about 0.63. These values are close to unity which is consistent with that observed by Shah (2008) in the separated and reattachment regions of turbulent flows over ribs in a ZPG at Re_h of 2640. In the present study and prior separated and reattached turbulent flows (Ismail, 1999; Shah, 2008), the peak values may be close to unity but there is a high level of anisotropy throughout the flow.

The Townsend's structure parameter is an important parameter used for calibrating turbulence models. Harsha and Lee (1970) proposed a constant value of $-uv/(2k) = 0.15$ while a constant value of $-uv/2k = 0.12$ was recommended by Launder *et al.*, (1975). In the present study, the magnitude of the structure parameter rises from zero at the wall and peaks at 0.15 but declines towards the freestream. Shah (2008) observed a maximum value of 0.2 in the separated and reattachment regions of turbulent flow over ribs in a ZPG at $Re_h = 2640$, which is about 25% higher than that observed in the present study but the distribution is similar to that observed in this study. The distribution observed in the present study and prior separated and reattached turbulent flows indicates that the use of a constant value of 0.15 in turbulence models will lead to inaccuracies in predicting separated and reattached turbulent flows.

4.2.5 Turbulence energy production

The sustainability of turbulence energy is dependent on the rate of production of new eddies to replace those lost by viscous dissipation. The rate of turbulence production for a two dimensional turbulent flow is given by:

$$P_k = \left\{ -uv \left(\frac{\partial u}{\partial y} + \frac{\partial v}{\partial x} \right) - u^2 \left(\frac{\partial u}{\partial x} \right) + v^2 \left(\frac{\partial v}{\partial x} \right) \right\}$$

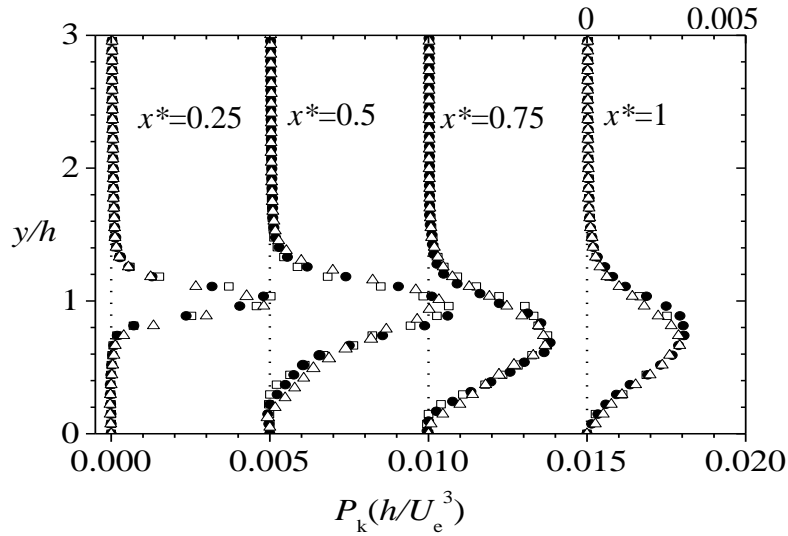


Figure 4.11: Turbulence production at various streamwise locations in the separated and reattachment regions. Symbols: \square SM \triangle WM \bullet SG

In canonical near wall turbulent flows, it has been demonstrated that $-uv \left(\frac{\partial U}{\partial y} \right)$ is the major contributor to turbulence production and that the rate of turbulence energy production can be approximated as $P_k = -uv \left(\frac{\partial U}{\partial y} \right)$. In the present study, the rate of the turbulence production was determined from both the exact and the approximated equations of P_k . Significant difference was not observed between the two data sets. This may be attributed to the contribution from the normal stress terms being comparable in magnitude and having opposite signs which make their sum negligible. The profiles for the approximate values ($P_k \approx -uv \left(\frac{\partial U}{\partial y} \right)$) are shown in Figure 4.11 because the data quality was better than profiles obtained using the exact expression.

At the selected streamwise locations, surface roughness has no significant effect on turbulence energy production. Consistent with prior studies (Kasagi and Matsunaga, 1995; Le *et al.*, 1997; Shah, 2008), turbulence energy production level is enhanced in the flow region of strong shear layer in the separated region. However at $x^* = 0.5$, where the maximum peak of turbulence production

occurs, the maximum peak value observed for the production in the present study is 0.006 which is about 50% less than that observed by Kasagi and Matsunaga (1995) in turbulent flows over BFS with ZPG and Shah (2008) in turbulent flows over ribs with ZPG. Nakagawa and Nezu (1987) at similar location observed 0.013 for turbulent flows over BFS in open channel and Agelinchaab and Tachie (2008) observed a value of 0.004, 0.006 and 0.01 respectively for triangular, semicircular and square prisms in open channel. The disparity in the results should be expected since there was variation in the magnitude of the Reynolds stress maxima as discussed in section 4.2.2.

4.2.6 Triple velocity correlation

The distribution of triple velocity correlation is presented in this section. These quantities are important because their gradients are related to turbulence diffusion in the turbulent kinetic energy and Reynolds stress equations. For a two dimensional flow, the turbulence diffusion term in the turbulent kinetic energy and Reynolds stress equations is given by:

$$\frac{\partial(u^3 + uv^2 + uw^2)}{\partial x} + \frac{\partial(u^2v + v^3 + vw^2)}{\partial y}$$

Since the spanwise fluctuation could not be measured, the diffusion term was approximated as follows:

$$\frac{\partial(u^3 + uv^2)}{\partial x} + \frac{\partial(u^2v + v^3)}{\partial y}$$

To have a meaningful understanding of the contribution of the triple velocity correlation to turbulence diffusion, the distribution of the streamwise flux ($u^3 + uv^2$) and the wall normal flux ($v^3 + u^2v$) are presented instead of the conventional u^3 , v^3 and u^2v and uv^2 . The normalized streamwise flux is presented in Figure 4.12(a) whereas the normalized wall normal flux is presented in Figure 4.12(b). The components of the streamwise flux ($u^3 + uv^2$) have same trend along the wall normal axis and those

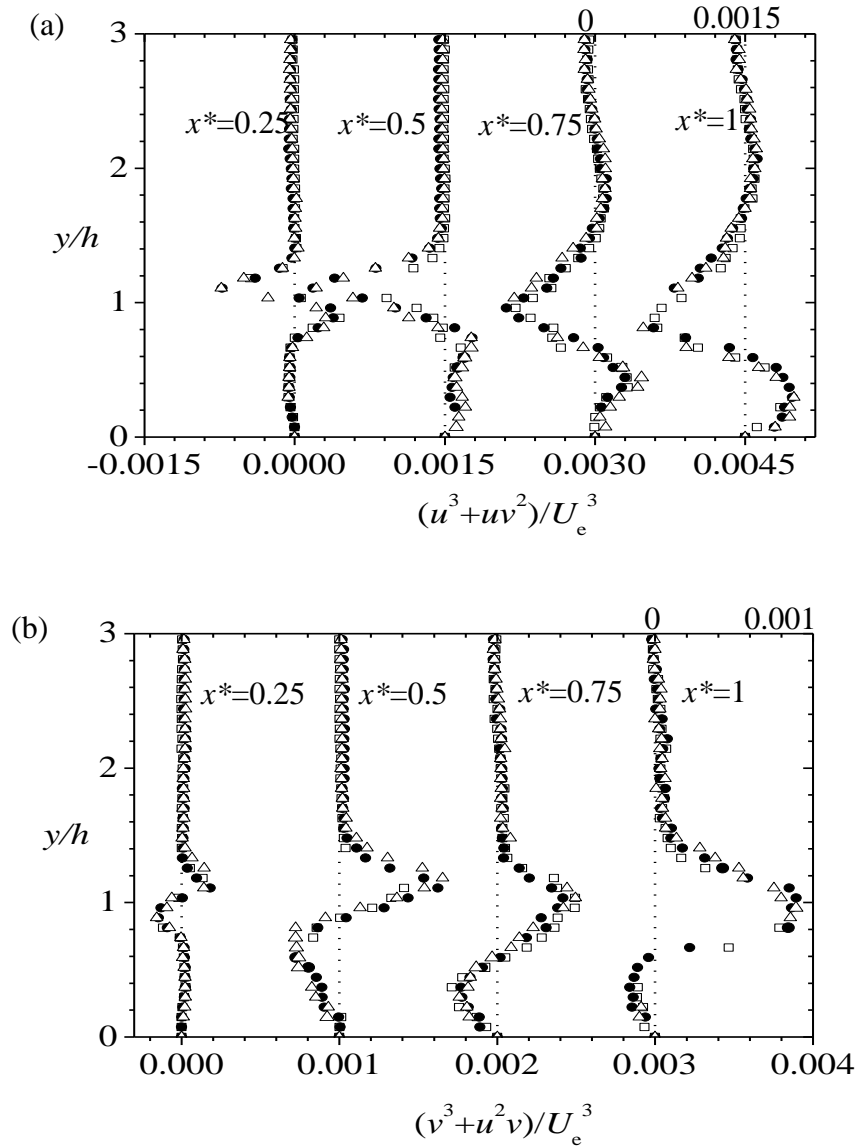


Figure 4.12: Triple velocity correlation: (a) streamwise flux (b) wall normal flux at various streamwise locations in the separated and reattachment regions. Symbols: \square SM \triangle WM \bullet SG

of the wall normal flux $(v^3 + u^2v)$ also have same trend along the wall normal axis. This observation agrees with results presented by Driver and Seegmiller (1985) for separated and reattached turbulent flow downstream of a BFS with ZPG and by Shah (2008) for separated and reattached turbulent flow downstream of a rib with ZPG. It should be noted that u^3 has the highest magnitude among the four triple velocity correlation components. This contributes significantly to the magnitude of the streamwise flux thereby making it higher than the magnitude of the wall normal flux.

No significant surface roughness effect was observed for the profiles at the various streamwise locations presented for both the streamwise and wall normal fluxes. Distribution of streamwise and wall normal fluxes in the present study gives the indication that turbulence diffusion in separated and reattached turbulent flows may not be negligible compared to other terms in the transport equations as in the case of canonical near wall turbulent flows and open channel turbulent flows.

4.3 Flow characteristics in the recovery region

The characteristics of the flow in the recovery region are presented in this section. This section consists of three subsections. The first subsection discusses surface roughness effect on the distribution of the mean and turbulent quantities. The second subsection discusses the recovery process of the flow whereas the third subsection examines surface roughness effects on the coherent structures using a two point spatial correlation function. As indicated earlier in section 2.2, in canonical near wall turbulent flows, the inner region of the boundary layer is scaled on the friction velocity (U_τ) and viscous length (ν/U_τ) whereas the outer region of the boundary layer is scaled on the freestream velocity (U_e) and the boundary layer thickness (δ). The outer scales were adopted to scale the quantities in the recovery region. This is because of the uncertainty in the determination of U_τ using the Clauser plot technique where the streamwise mean velocity data is forced to fit the classical logarithmic law.

It should be noted that, for the outer scales, the local freestream streamwise mean velocity (U_e) and the local boundary layer thickness (δ) were used as the velocity scale and the length scale respectively. The values of U_e and δ obtained at the selected streamwise locations where data are presented in this section are shown in Figure 4.13(a) and Figure 4.13(b) respectively. The locations at which profiles of the mean

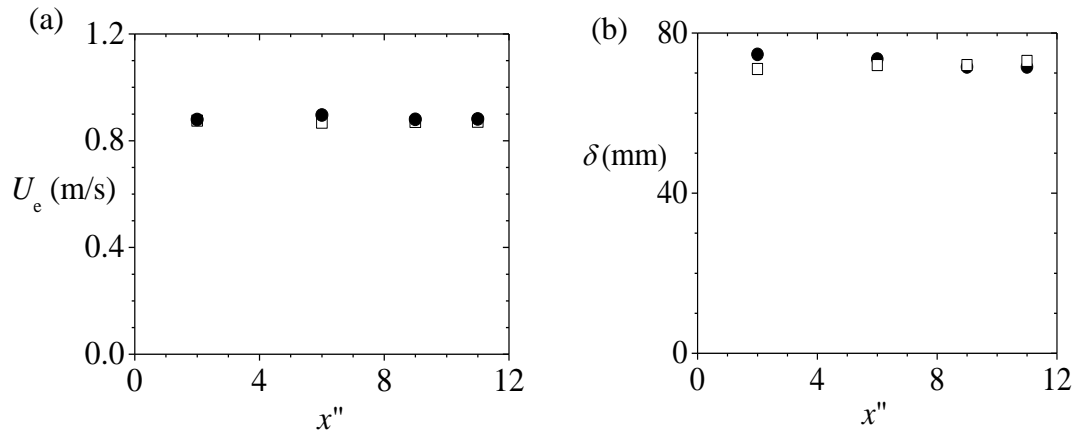


Figure 4.13: (a) Local freestream streamwise mean velocity (b) local boundary layer thickness at selected streamwise locations in the recovery region Symbols: \square SM \bullet SG

and turbulent quantities are presented are $x'' = x'/x_r = 2, 6, 9$ and 11 , where x' is the streamwise distance beyond the reattachment point. These locations correspond to $x'/h \approx 10, 30, 45$ and 55 respectively. The profiles presented in this section are for only *SM* and *SG* because no significant difference was observed between *SM* and *WM*.

4.3.1 Roughness effects on mean and turbulent statistics in the recovery region

4.3.1.1 Streamwise mean velocity

Profiles of the streamwise mean velocity at $x'' = 2, 6$, and 11 are presented in Figure 4.14. These locations are the same for subsequent profiles that are presented in this subsection. It is apparent that as the flow evolves along the streamwise distance, the profiles become more uniform. Surface roughness effect on U was obvious at $x'' = 11$ in the near wall region. At this location, the sand grain roughness is observed to cause the magnitude of the normalized streamwise mean velocity to be less than that of the smooth surface from the wall up to $y/\delta = 0.1$. This implies that the mean flow begins to experience higher resistance caused by the sand grain roughness.

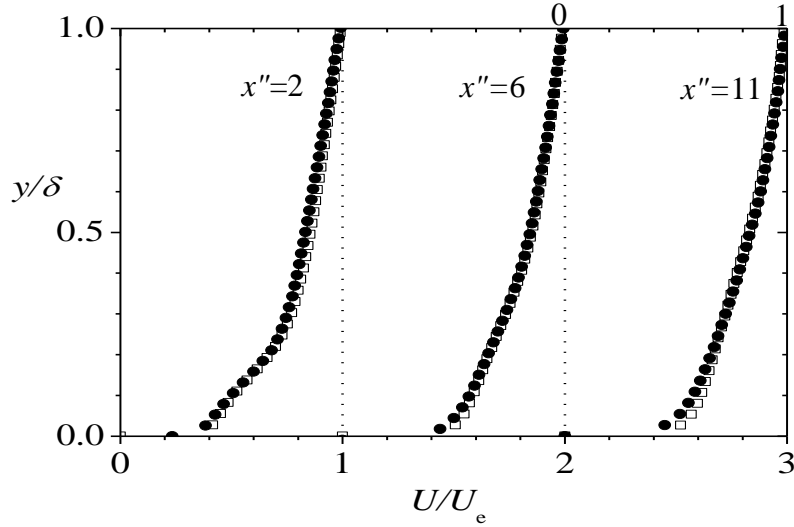


Figure 4.14: Profiles of streamwise mean velocity in the recovery region. Symbols: \square SM \bullet SG

4.3.1.2 Reynolds stresses

The distributions of the Reynolds stresses at the selected streamwise locations are presented in Figure 4.15 (a-c). Beyond the reattachment point, the magnitude of the Reynolds stresses decays. This gives the indication that the large scale eddies that were carried into the recovery region from the separated shear layer, are gradually decaying due to the spreading and mixing of the new boundary layer. This observation is consistent with prior results obtained in separated and reattached turbulent flow (Jovic, 1996; Shah, 2008). Unlike the streamwise mean velocity, the streamwise Reynolds normal stress (u^2/U_e^2) showed surface roughness effect at $x'' = 6$ and 11 in the near wall region. For example, for $x'' = 6$ at $y/\delta = 0.07$, SG profile shows an increase of 22% and for $x'' = 11$ at $y/\delta = 0.07$, SG profile shows increase of 25%.

The wall normal Reynolds stress showed roughness effect at $x'' = 11$. SG profile was about 12% higher in magnitude than SM from the wall up to $y/\delta = 0.13$. Similar to u^2/U_e^2 , $-uv/U_e^2$ showed roughness effects at $x'' = 6$ and 11. SG profile was about 22% higher in magnitude than SM profile from the wall up to $y/\delta = 0.18$. The significant

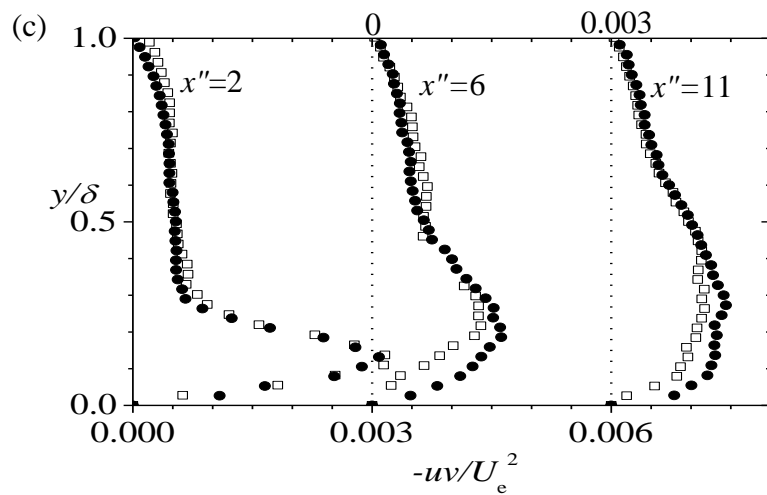
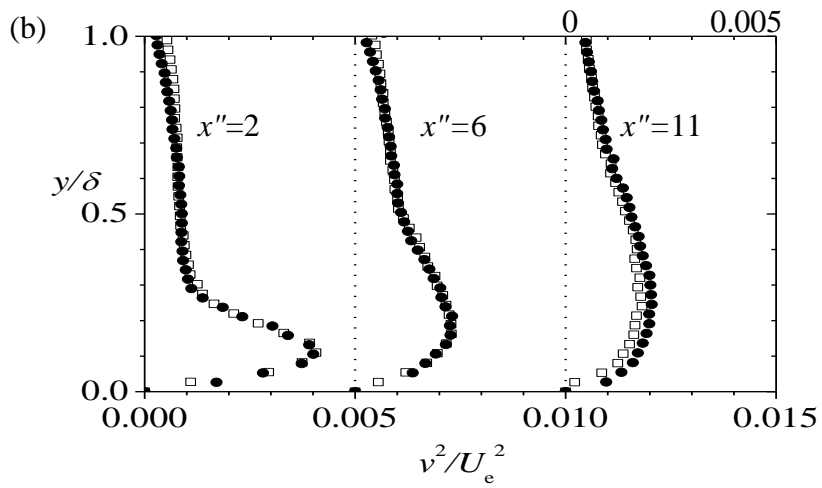
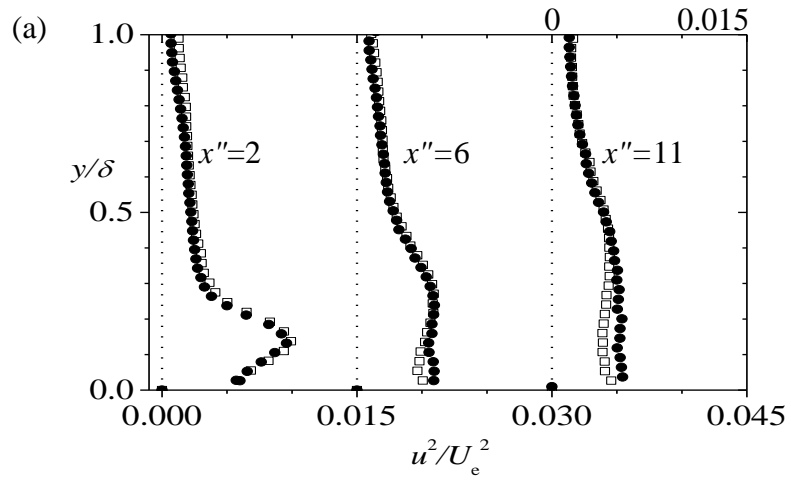


Figure 4.15: Profiles of Reynolds stresses in the recovery region: (a) u^2/U_e^2 (b) v^2/U_e^2 (c) $-uv/U_e^2$. Symbols: \square SM \bullet SG

increase in the levels of the Reynolds stresses caused by surface roughness effects is consistent with surface roughness effects on Reynolds stresses in canonical near wall turbulent flows (Schultz and Flack, 2007) and open channel turbulent flows (Tachie *et al.*, 2003)

4.3.1.3 Turbulence kinetic energy

The profiles for the turbulence kinetic energy for the various streamwise locations in the recovery region are presented in Figure 4.16. Similar to the Reynolds stress profiles, the magnitude of the turbulence kinetic energy decays beyond the reattachment point. Also up to $y/\delta = 0.2$ at $x'' = 11$, SG significantly increased the turbulence kinetic energy by about 18% compared to the smooth wall profile.

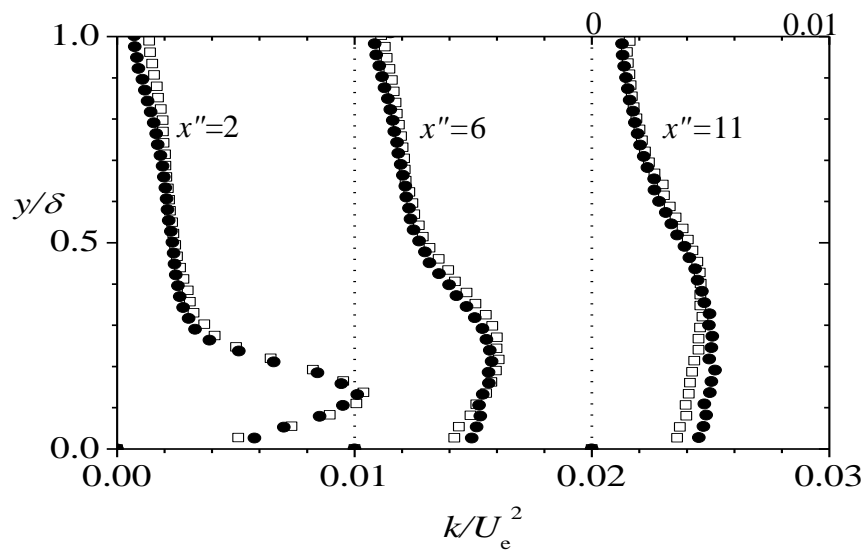


Figure 4.16: Profiles of turbulence kinetic energy in the recovery region. Symbols: \square SM \bullet SG

4.3.1.4 Reynolds stress ratios

The profiles for the ratio of the Reynolds normal stresses (v^2/u^2) and the Townsend structure parameter in the recovery region at the selected streamwise locations are presented in Figure 4.17(a) and Figure 4.17(b) respectively. Irrespective of the surface condition, the distribution of v^2/u^2 rises from zero at the wall and remains almost

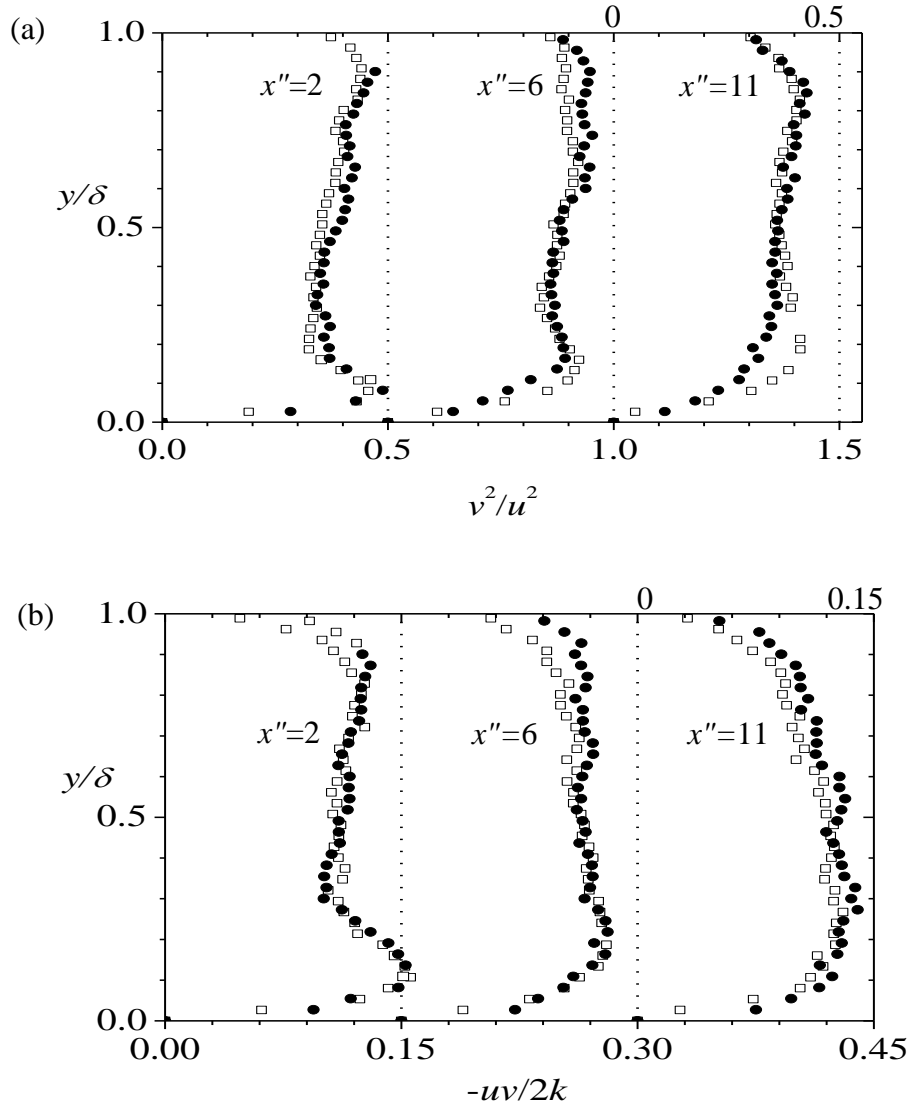


Figure 4.17: Reynolds stress ratios in the recovery region; (a) v^2/u^2 (b) $-uv/2k$. Symbols: $\square SM$ $\bullet SG$

constant at 0.4 in the region $y/\delta > 0.2$. As shown in Figure 4.17(a), surface roughness effect on v^2/u^2 is significant at $x'' = 11$ in the near wall region, specifically from the wall up to $y/\delta = 0.2$. The profiles for the Townsend structure parameter are presented in Figure 4.17(b). Significant surface roughness effect on the profiles was not discerned. In the early recovery region, at $x'' = 2$, a maximum value of 0.15 was observed which is the same as that observed in the separated and reattachment regions. Further downstream (at $x'' = 6$ and 11), a maximum value of 0.12 was observed.

4.3.1.5 Triple velocity correlation

The distributions of the streamwise and the wall normal fluxes of the triple velocity correlations are presented in Figure 4.18. The streamwise flux and the wall normal flux are presented in Figure 4.18(a) and Figure 4.18(b) respectively. Surface roughness did not cause any significant difference in the profiles at the various streamwise locations. However, the negative and positive lobes exhibited by the

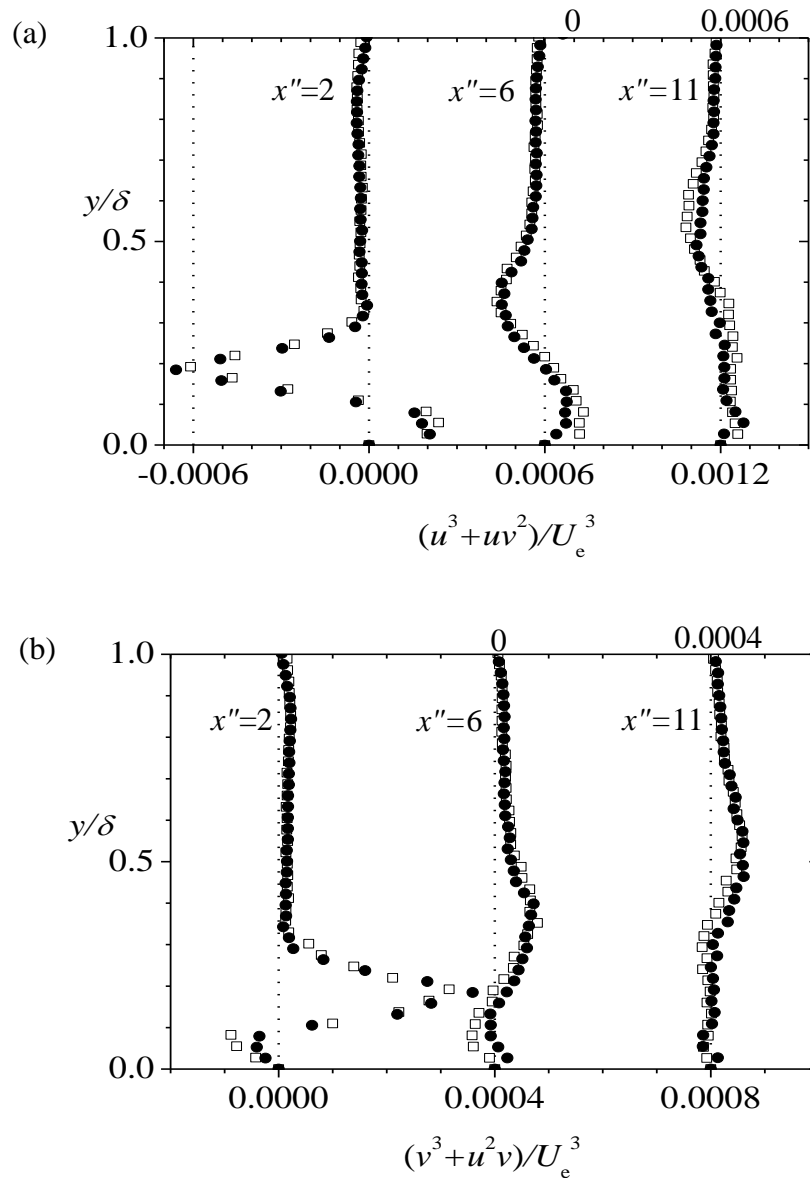


Figure 4.18: Triple velocity correlation in the recovery region (a) streamwise flux (b) wall normal flux. Symbols: \square SM \bullet SG

streamwise flux and the wall normal flux in the near wall region in the separated and reattachment regions diminish as the flow evolves in the streamwise direction in the recovery region. This is because, the large scale eddies which contribute to turbulence diffusion decay rapidly close to the wall after the reattachment of the flow.

4.4 Roughness effects on the flow recovery process

The recovery of the flow from intense turbulence generated in the separated region is a gradual process in both the streamwise and wall normal directions. This is observed in previous studies to be influenced by factors such as freestream turbulence and geometry for inducing flow separation. This section therefore presents effect of surface roughness on the recovery process. Surface roughness effect on the recovery process was examined through the distribution of the streamwise mean velocity and the Reynolds stresses. The locations at which profiles of these quantities are presented are $x'' = 6, 9$ and 11 . The streamwise mean velocity profiles for *SM* and *SG* are shown in Figure 4.19(a) and Figure 4.19(b) respectively. In these figures and subsequent figures presented in this section, data points were skipped to avoid overcrowding of the data. Figure 4.19(a) shows that the magnitude of the profiles for *SM* shown for $x'' = 6$ in the near wall region is significantly different from that observed for the profiles at $x'' = 9$ and 11 . For example at $y/\delta = 0.07$, the magnitude of *SM* at $x'' = 6$ is 4% significantly higher than that obtained at $x'' = 9$ and 11 . In Figure 4.19(b) the difference in the profiles over *SG* at the three locations presented shows no significant difference. This observation gives the indication that *SG* promotes self-similarity of the streamwise mean velocity earlier than *SM* in the recovery region.

The streamwise Reynolds stress profiles over *SM* and *SG* are shown in Figure 4.19(c) and Figure 4.19(d) respectively. At $y/\delta \leq 0.5$ in Figure 4.19(c), *SM* profile shows a

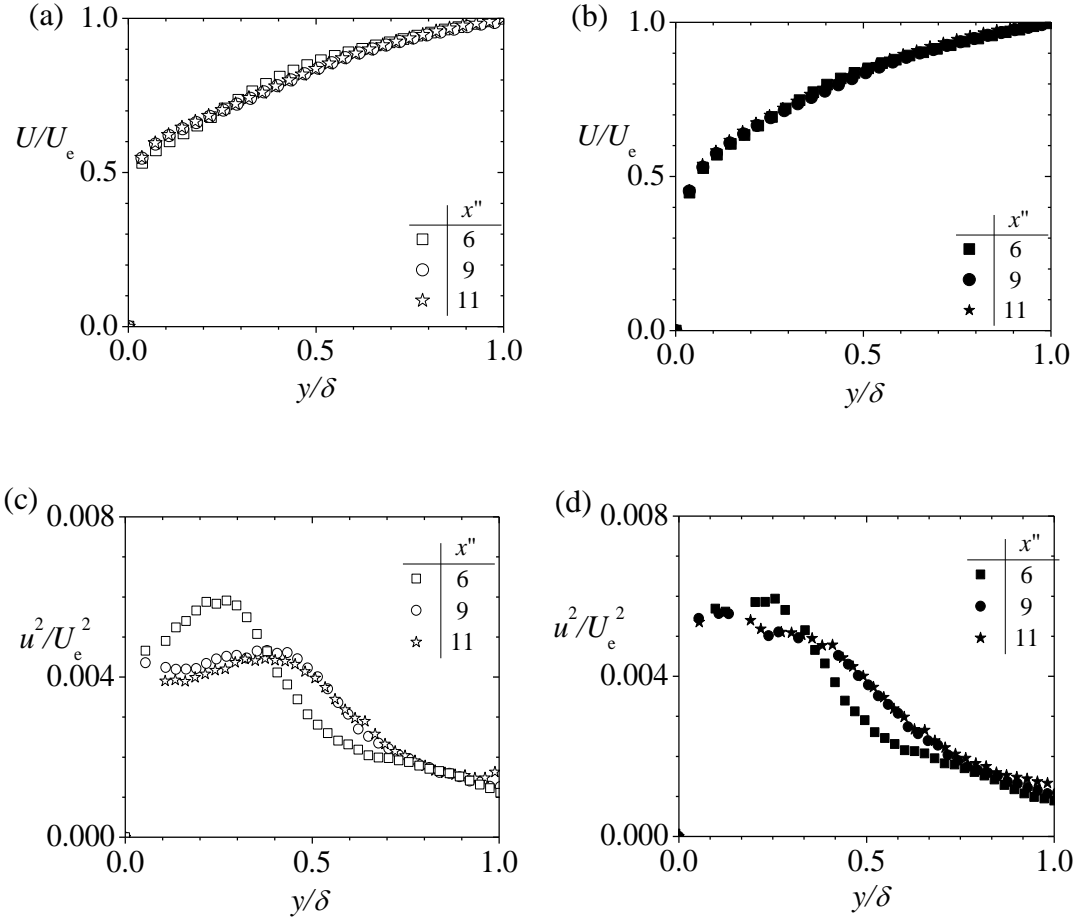


Figure 4.19: Distribution of streamwise mean velocity (a) *SM* (b) *SG*; distribution of streamwise Reynolds normal stress (c) *SM* and (d) *SG*

moderate decrease of about 7% in the magnitude of the profiles from $x'' = 9$ to $x'' = 11$. This difference is comparable to a measurement uncertainty of 10%. Meanwhile, the profiles of *SG* at $x'' = 9$ and 11 are almost indistinguishable. Similar to the streamwise Reynolds normal stress, there is no significant difference in the magnitude of the profiles for the wall normal Reynolds normal stress (as shown in Figure 4.20(a-b)) and the Reynolds shear stress (as shown in Figure 4.20(c-d)) at $x'' = 9$ and 11 for both *SM* and *SG*. The observation made for the distribution of the Reynolds stresses indicates that the turbulence field has attained self-similarity.

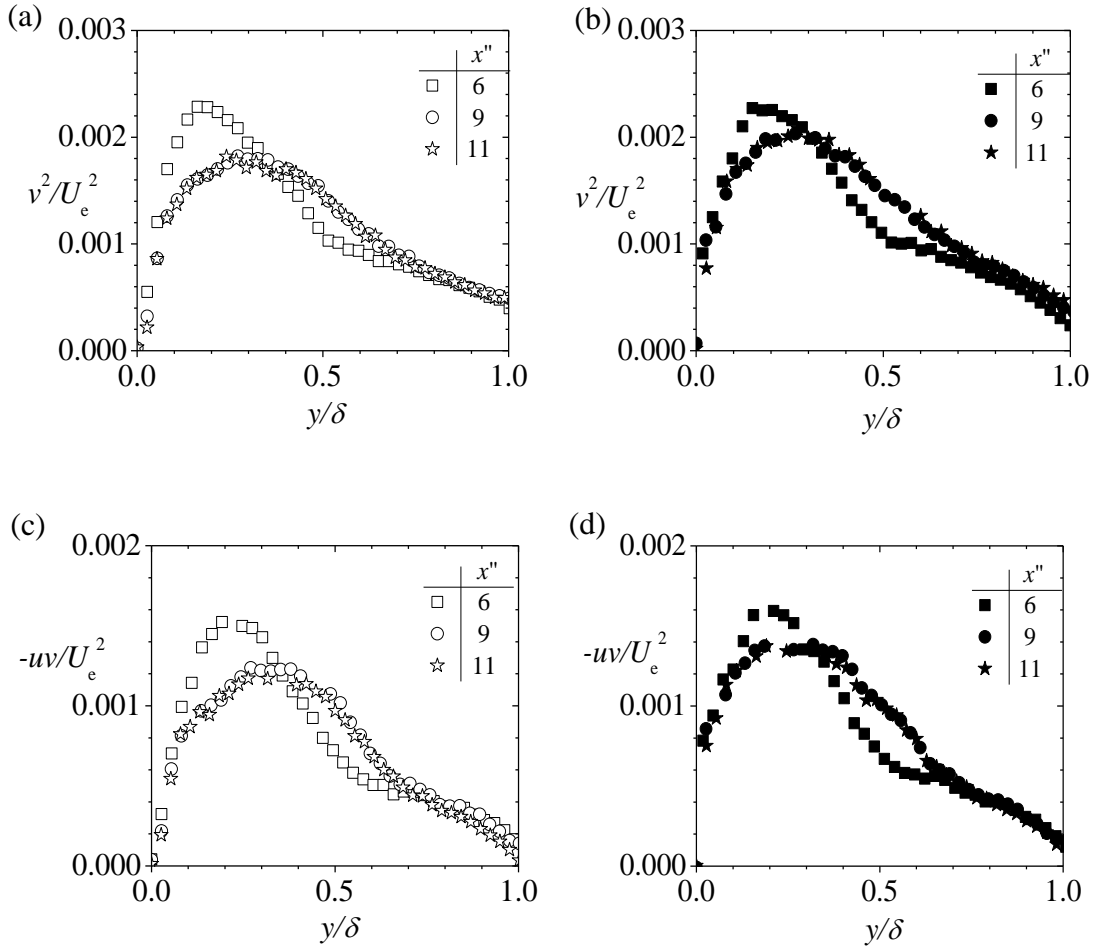


Figure 4.20: Distribution of streamwise Reynolds normal stress (a) *SM* and (b) *SG*; distribution of Reynolds shear stress (c) *SM* and (d) *SG*

4.5 Two point correlation analysis

Two-point correlation analysis was employed in the present study to examine the effect of surface roughness on the average spatial extent of the hairpin packets which is made up of series of hairpin vortices in the recovery region. The two point correlations have been used in previous near wall turbulent flows to study the features of the hairpin packets (Christensen and Wu, 2005; Volino *et al.*, 2007). The two-point correlation coefficients in the x - y plane are given by:

$$R_{ij}(x_{ref} + \Delta x, y_{ref} + \Delta y) = \frac{u'_i(x_{ref}, y_{ref}) u'_j(x_{ref} + \Delta x, y_{ref} + \Delta y)}{\sigma_i(x_{ref}, y_{ref}) \sigma_j(x_{ref} + \Delta x, y_{ref} + \Delta y)}$$

where u_i' and u_j' are the fluctuating velocity components, Δx is the spatial separation in the streamwise direction, Δy is the spatial separation in the wall normal direction, x_{ref} is the streamwise reference location, y_{ref} is the wall normal reference location and σ_i and σ_j are root-mean-squares of the i^{th} and j^{th} velocity components.

Two point correlation analysis was done in the recovery region at $x'' = 2$ and 11. Iso-contours of the streamwise correlation coefficient (R_{uu}) and wall normal correlation coefficient (R_{vv}) were obtained at $x'' = 2$ and 11 at $0 \leq y_{ref}/\delta \leq 1$ to determine the average spatial extent of the hairpin packets. Typical contour plots of R_{uu} and R_{vv} obtained at $x'' = 11$ for *SM* and *SG* with the correlation centered at

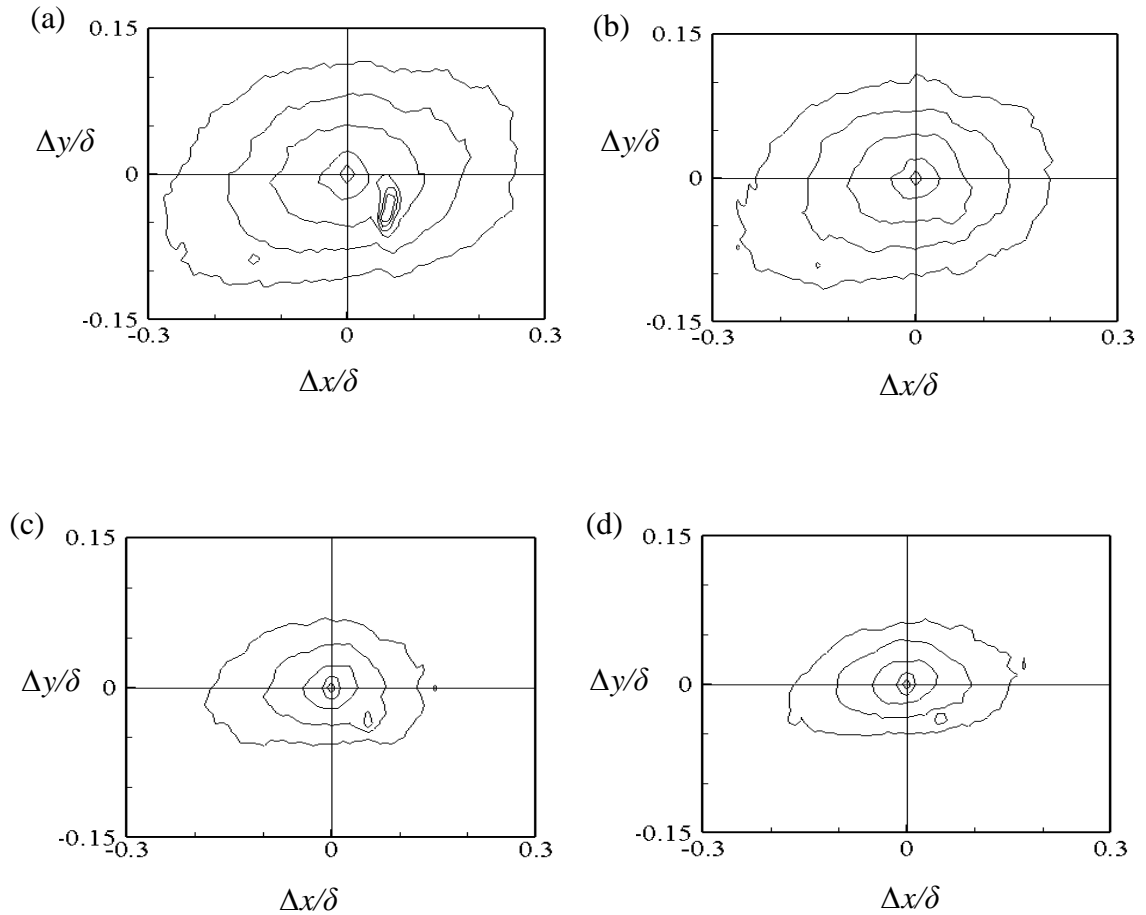


Figure 4.21: Contours of R_{uu} at $x'' = 11$: centered at $y/\delta = 0.2$ (a) *SM* and (b) *SG*; centered at $y/\delta = 0.6$ (c) *SM* and (d) *SG*; outermost contour $R_{uu} = 0.5$, contour spacing = 0.1.

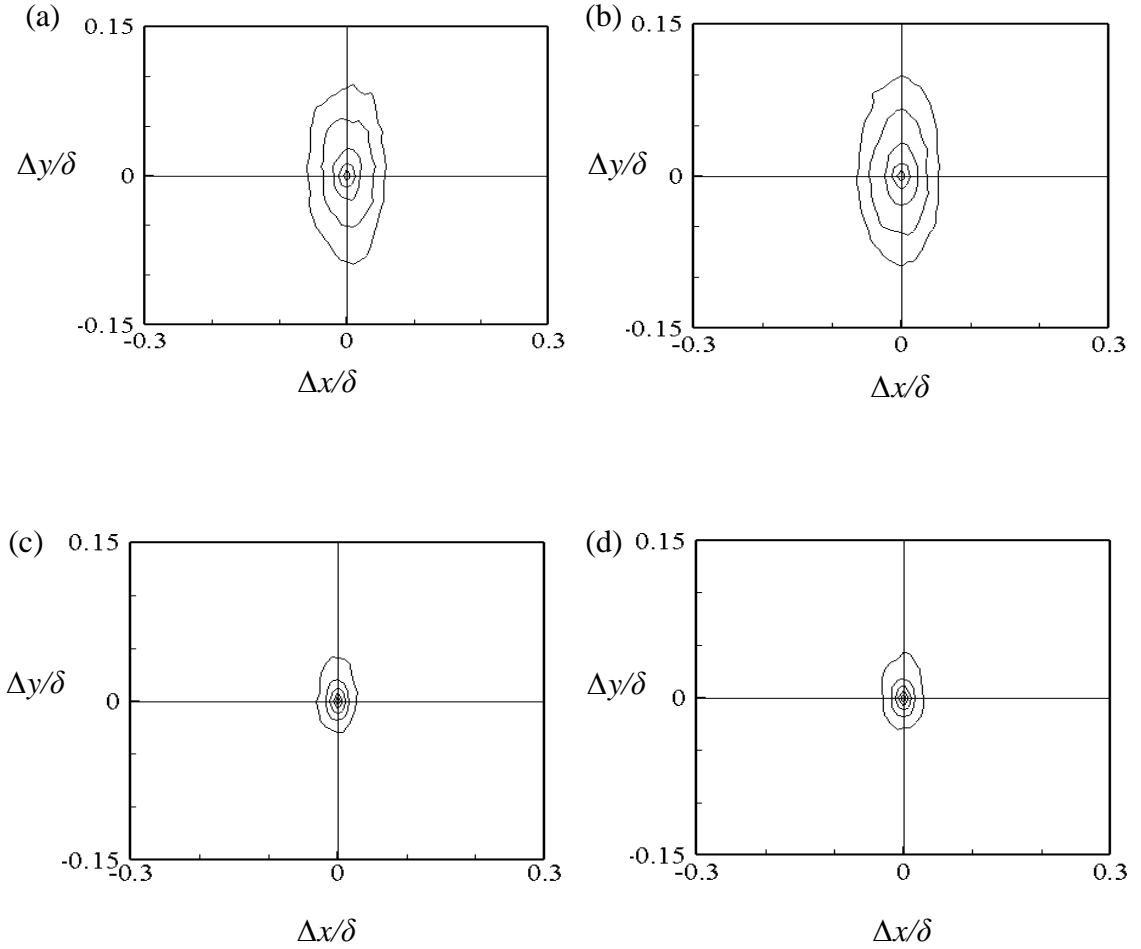


Figure 4.22: Contours of R_{vv} at $x'' = 11$: centered at $y/\delta = 0.2$ (a) *SM* and (b) *SG*; centered at $y/\delta = 0.6$ (c) *SM* and (d) *SG*; outermost contour $R_{vv} = 0.5$, contour spacing = 0.1.

$y_{ref}/\delta = 0.2$ and 0.6 are shown in Figure 4.21 and Figure 4.22 respectively. The R_{vv} iso-contours are smaller in size and more rounded than the R_{uu} over both the smooth and rough walls.

From the R_{uu} iso-contour plots obtained at $x'' = 2$ and 11 correlated at $0 < y_{ref}/\delta \leq 1$, the streamwise extent (Lx_{uu}) and wall normal extent (Ly_{uu}) of the hairpin packets were determined using the methodology described by Christensen & Wu (2005) and Volino *et al.* (2007). The Lx_{uu} is defined as twice the distance from the self-correlation point to the most downstream location on the 0.5 contour level, while the Ly_{uu} is defined as the wall normal distance between points closest and farthest from the wall on the 0.5

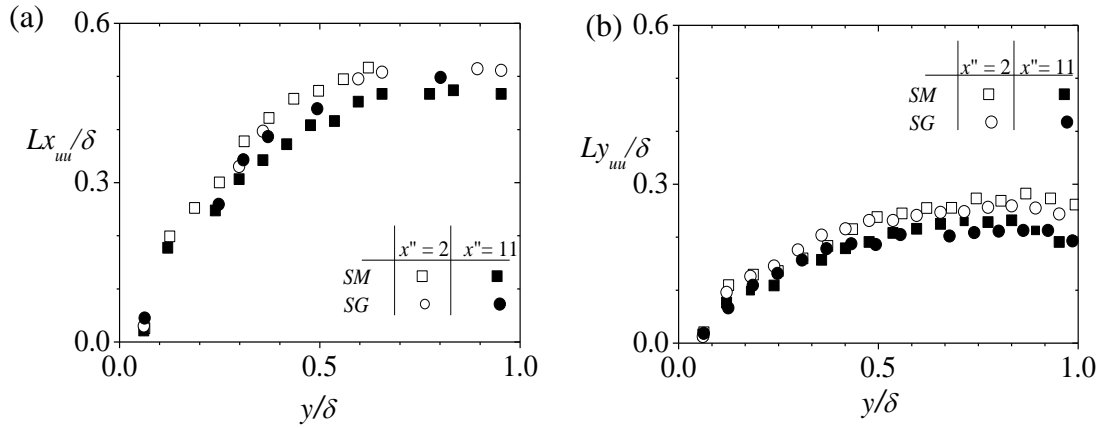


Figure 4.23: Extent of $R_{uu} = 0.5$ contour as a function of y/δ at $x'' = 2$ and 11: (a) streamwise extent (b) wall normal extent

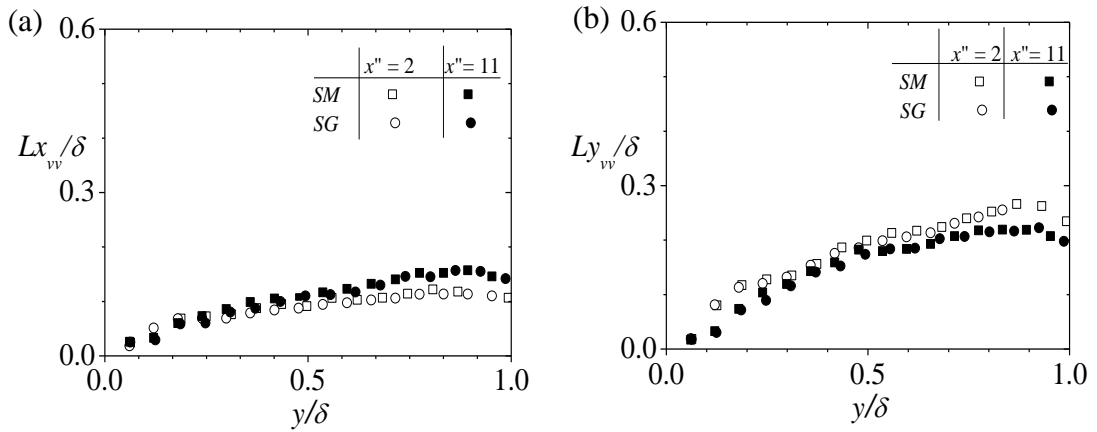


Figure 4.24: Extent of $R_{vv} = 0.5$ contour as a function of y/δ at $x'' = 2$ and 11: (a) streamwise extent (b) wall normal extent

contour level. The distribution of the streamwise extent and wall normal extent for R_{uu} is shown in Figure 4.23(a) and Figure 4.23(b) respectively. Surface roughness shows no significant effect on the streamwise and wall normal extents of R_{uu} . The streamwise and wall normal extent of R_{uu} show that the hairpin packets grow gradually from the wall and attain a maximum value at about $y/\delta = 0.7$. The peak values obtained for the streamwise extent are 0.51 and 0.47 respectively at $x'' = 2$ and 11. At $x'' = 2$, the streamwise extent shows values higher than that at $x'' = 11$ from $y/\delta = 0.3$. However, within measurement uncertainty of 10%, this difference is

insignificant. The trend of the wall normal extent is similar to that observed for the streamwise extent but with magnitude less than the streamwise extent. The magnitude of the peak values at $x'' = 2$ and 11 are 0.25 and 0.23 respectively.

From the R_{vv} contour plots at the various self-correlation points, the streamwise (Lx_{vv}) and wall normal extents (Ly_{vv}) of the hairpin packets were also determined using the methodology described by Christensen & Wu (2005) and Volino *et al.*, (2007). Lx_{vv} is defined as the streamwise distance between the most upstream and downstream points on the 0.5 contour level and Ly_{vv} is defined as the wall normal distance between the points closest and farthest from the wall on the 0.5 contour level. The distribution of the streamwise and wall normal extents for R_{vv} is shown in Figure 4.25(a) and Figure 4.25(b) respectively. Similar to R_{uu} , the streamwise and wall normal extents of R_{vv} show that the hairpin packets grow gradually from the wall but attain their peak close to the boundary layer edge at about $y/\delta = 0.9$. The distribution of the streamwise and wall normal extent of R_{vv} do not exhibit significant surface roughness effects. The magnitude obtained for the streamwise extent for R_{vv} is less than that of the R_{uu} by about 68% whereas the magnitude of the wall normal extent for R_{vv} compares reasonably with that of the R_{uu} wall normal extent. As the flow evolves in the streamwise direction, the distribution of the streamwise extent at $x'' = 2$ is about 25% less than that of the streamwise extent at $x'' = 11$. For the wall normal extent, the distribution shows that at $x'' = 2$, the wall normal extent is about 15% significantly higher than that of the wall normal extent at $x'' = 11$.

CHAPTER 5

CONCLUSIONS AND RECOMMENDATIONS FOR FUTURE WORK

5.1 Conclusions

The research presented in this thesis was conducted to study the effects of surface roughness on the dynamics of turbulent flow downstream of a backward facing step in an open channel. Two rough surfaces (wire mesh grit-80 and sand grains of average diameter 1.5 mm) were studied in addition to a reference smooth surface. Particle image velocimetry technique was used to measure the velocity field and results were presented up to 60 step heights downstream of the step. The results from this study demonstrated that:

- The growth of vorticity thickness in the separated shear layer was linear with no significant surface roughness effect.
- The reattachment length for the separated shear layer was not significantly affected by surface roughness.
- The mean flow pattern of the recirculation region was similar for the smooth and rough surfaces studied.
- The distribution of the mean and turbulent quantities studied in the separated and the reattachment regions of the flow did not exhibit significant surface roughness effects but indicated that in these regions, the mean and turbulent quantities are significantly enhanced compared to canonical near wall turbulent flows and open channel turbulent flows.
- In the separated and reattachment regions, the flow is highly anisotropic and that turbulence models assuming local isotropy will not predict the flow in this category accurately.

- In the recovery region, significant surface roughness effect is observed beyond 35 step heights from the trailing edge of the BFS. However, it was revealed that the type of roughness element used will affect the flow dynamics differently.
- Sand grain roughness promotes self-similarity of the flow in the recovery region earlier than the smooth surface.
- Surface roughness showed no significant effect on the average extent of the hairpin packets obtained from the streamwise and wall normal fluctuating velocity contours in the recovery region.

5.2 Recommendations for future work

Based on the findings of this study, it is recommended that:

- Wide range of roughness elements should be studied to establish the universality of the findings on surface roughness effects in the present study.
- In order to confirm surface roughness effects on the recovery of the flow towards a near wall turbulent boundary layer, the dynamics of the flow should be studied beyond 60 step heights.

REFERENCES

- Adams, E.W. and Johnston, J.P. 1988. Effects of the separated shear layer on the reattachment flow structure. *Exp. Fluids*. 6: 493– 499.
- Afzal, B., Al Faruque, M. and Balachandar, R. 2009. Effect of Reynolds number, near-wall perturbation and turbulence on smooth open-channel flows. *J. Hydraulic Research*. 47: 66-81.
- Agelinchaab, M. and Tachie. M.F. 2008. PIV study of separated and reattached open channel flow over surface mounted blocks. *J. Fluids Eng.* 130: 1-9.
- Barri1, M.G. El Khoury, K., Andersson H.I., and Pettersen, B. 2010. DNS of backward-facing step flow with fully turbulent inflow. *Int. J. Numerical Methods in Fluids*. 64: 777–792.
- Brown, G.L. and Roshko. A. 1974. On density effects of large structures in turbulent mixing layers. *J. Fluid Mech.* 64: 775–816.
- Castro, I.P. and Epik, E. 1998. Boundary layer development after a separated region. *J. Fluid Mech.*, 374: 91-116.
- Ching, C.Y., Djenidi L. and Antonia R.A. 1995. Low- Reynolds-number effects in a turbulent boundary layer. *Exp. Fluids*. 19: 61- 68.
- Christensen, K.T. and Wu. Y. 2005. Characteristics of vortex organization in the outer layer of wall turbulence. *Proceedings of Fourth International Symposium on Turbulence and Shear Flow Phenomena*. 3: 1025–1030.
- Coleman, H.W. and Steele, W.G. 1995. Engineering application of experimental uncertainty analysis. *AIAA Journal*. 33: 1888 - 1896.

- Coles, D.E. 1956. The law of the wake in the turbulent boundary layer. *J. Fluid Mech.* 1: 191–226.
- Djenidi, L., Antonia, R.A., Amielh, M.L. and Anselmet, F. 2008. A turbulent boundary layer over a two-dimensional rough wall. *Exp. Fluids.* 44:37–47.
- Djilali, N. and Gartshore. I. S. 1991. Turbulent flow around a bluff rectangular plate. Part I: Experimental investigation. *J. Fluids Eng.*, 113:51–59.
- Driver, D.M. and Seegmiller, H.L. 1985. Features of a Reattaching Turbulent Shear Layer Subject to an Adverse Pressure Gradient. *AIAA Journal.* 82: 1029-1044.
- Eaton, J.K. and Johnston. J.P. 1981. A Review of research on subsonic turbulent flow reattachment. *AIAA Journal.* 19: 1093–1100.
- Fernholz, H.H. and Finley, P.J. 1996. The incompressible zero-pressure-gradient turbulent boundary layer: an assessment of the data. *Aerospace Sci.* 32: 245-311.
- Gad-el-Hak, M. and Bandyopadhyay, P.R. 1994. Reynolds number effects in wall-bounded turbulent flow. *App. Mech. Rev.* 47: 307–64.
- George, W.K. and Castillo, L. 1997. Zero-pressure-gradient turbulent boundary layer. *App. Mech. Rev.* 50: 689-729.
- Harsha, P.T and Lee, S.C. 1970. Correlation between Turbulent Shear Stress and Turbulent Kinetic Energy. *AIAA Journal.* 8: 1508-1510.
- Ismail B.C. 1999. Introductory turbulence modelling. Lecture notes. Department of Mechanical and Aerospace Engineering, West Virginia University.
- Jovic, S. 1996. An experimental study of a separated and reattached flow behind a backward facing step, $Re_h = 37000$. *NASA Technical Memorandum*, 110384: 1-94.

- Kasagi, N. and Matsunaga A. 1995. Three-dimensional particle tracking velocimetry measurement of turbulence statistics and energy budget in a backward-facing step flow. *Int. J. Heat and Fluid Flow*. 16: 477- 485.
- Kim, B.N. and Chung, M.K. 1994. Experimental study of roughness effects on the separated flow over backward-facing step. *AIAA Journal*. 33: 159 - 161.
- Kostas, J., Soria, J. and Chong. M. S. 2002. Particle image velocimetry measurements of a backward-facing step flow. *Exp. Fluids*. 33: 838–853.
- Krogstad P-Å. and Antonia R.A. 1999. Surface roughness effects in turbulent boundary layers. *Exp. Fluids*. 27: 450-460.
- Launder, B.E., Reece, G.J. and Rodi, W. 1975. Progress in Development of a Reynolds-stress turbulence model closure. *J. Fluid Mech*. 68: 537-566.
- Le, H., Moin, P. and Kim, J. 1997. Direct numerical simulation of turbulent flow over a backward-facing step. *J. Fluid Mech*. 330: 349-374.
- Mei, R., Adrian, R.J. and Hanratty, T.J. 1991. Particle dispersion in isotropic turbulence under Stokes drag and basset force with gravitational settling. *J. Fluid Mech*. 225: 481 – 495.
- Monkewitz, P.A., Chauhan, K.A. and Nagib, H.M. 2008. Comparison of mean flow similarity laws in zero pressure gradient turbulent boundary layers. *Phys. Fluids*. 20: 1-16.
- Nakagawa, H. and Nezu, I. 1987. Experimental investigation on turbulent structure of backward-facing step flow in an open channel. *J. Hydraulic Research*. 25: 67 – 88.

- Nezu, I. and Rodi, W. 1986. Open-channel flow measurements with a laser Doppler anemometer. *J. Hydraulic Eng.* 112: 335-355.
- Nikuradse J. (1933). *Strömungsgesetze in rauhen rohren, vdi-forsch.* (Engl. Transl. 1950. laws of flow in rough pipes. Naca Tm 1292.
- Ötügen, M.V. 1991. Expansion ratio effects on the separated shear layer and reattachment downstream of a backward-facing step. *Exp. Fluids.* 10: 273-280.
- Piirto, M., Saarenrinne, P., Eloranta, H. and Karvinen, R. 2003. Measuring turbulence energy with PIV in a backward-facing step flow. *Exp. Fluids.* 35: 219–236.
- Purtell. L.P., Klebanoff, P.S., Buckley, F. T. 1981. Turbulent boundary layer at low Reynolds number. *Phys. Fluids*, 24: 802–811.
- Raffel, M. Willert, C.E. and Kompenhans. J. 1998. *Particle image velocimetry: A practical guide.* Springer, New York.
- Schlichting, H. 1979. *Boundary layer theory.* 7th edition, McGraw-Hill, New York.
- Schultz, M.P. and Flack, K.A. 2007. The rough wall turbulent boundary layer from the hydraulically smooth to the fully rough regime. *J. Fluid Mech.* 580: 381–405.
- Shah, M.K. 2008. Effects of pressure gradient on two-dimensional separated and reattached turbulent flows. PhD Thesis. Department of Mechanical and Manufacturing Engineering. University of Manitoba.
- Sherry, M.J., Jacono D.L. Sheridan, J. 2009. Flow separation characterisation of a forward facing step immersed in a turbulent boundary layer. Sixth International

Symposium on Turbulence and Shear Flow Phenomena, Seoul, Korea, 22-24 June 2009. 1325-1330.

Simpson, R.L. 1989. Turbulent boundary-layer separation. *Ann. Rev. Fluid Mech.* 21: 205-234.

Song, S. and Eaton. J.K. 2002. The effects of wall roughness on the separated flow over a smoothly contoured ramp. *Exp. Fluids.* 33: 38–46.

Spalart, P.R. 1988. Direct simulation of a turbulent boundary layer up to $Re_\theta = 1410$. *J. Fluid Mech.* 187: 61–98.

Tachie, M.F. Balachandar, R. and Bergstrom. D. 2001. Open channel boundary layer relaxation behind a forward facing step at low Reynolds numbers. *J. Fluids Eng.* 123: 539-544.

Tachie, M.F., Balachandar, R. and Bergstrom D.J. 2003. Low Reynolds number effects in open channel turbulent boundary layers. *Exp. Fluids.* 34: 616–624.

Tay, G.F.K. 2009. Rough-wall turbulent flows in adverse and favourable pressure gradients. MSc. Thesis. Department of Mechanical and Manufacturing Engineering. University of Manitoba.

Volino, R.J. Schultz, M.P. and Flack. K.A. 2007. Turbulence structure in rough- and smooth-wall boundary layers. *J. Fluid Mech.*, 592: 263–293.

Westerweel, J., Draad, A.A., Th. Van der Hoeven, J.G. and Oord van, J. 1996. Measurement of fully developed turbulent pipe flow with digital particle image velocimetry. *Exp. Fluids.* 20: 165 – 177.

Wosnik, M., Castillo, L. and George W.K. 2000. A theory for turbulent pipe and channel flows. *J. of Fluid Mech.* 421: 1115–145.

Willert, C.E. and Gharib, M. 1991. Digital Particle Image Velocimetry. *Exp. Fluids.* 10: 181-193.